LA-UR-19-25386
Approved for public release; distribution is unlimited.

Title: Fracture Mechanics Analysis of Isotope Fuel Impact Tester, Milli-Watt, Multi-Hundred Watt and GPHS Outer Catch-Tube Subassembly Design

Author(s): Rodriguez, Edward A.

Intended for: Report

Issued: 2019-06-18 (rev.1)

Los Alamos NATIONAL LABORATORY EST 1943

J Division, Mail Stop P942, Los Alamos, NM 87545

RPT-J2-19-2481

Fracture Mechanics Analysis of Isotope Fuel Impact Tester, Milli-Watt, Multi-Hundred Watt and GPHS Outer Catch-Tube Subassembly Design

Edward A. Rodriguez, P.E.

May 30, 2019
LA-UR-19-25386

Preparer

Org	Name	Z#	Signature	Approval Date
J-2	Edward A. Rodriguez	110240	Edward A. Rodriguez	10 June 2019

Reviewers

Org	Name	Z#	Signature	Date
J-2	Kevin R. Fehlmann	327402	KEVIN FEHLMANN (Affiliate) Digitally signed by KEVIN FEHLMANN (Affiliate) Date: 2019.06.11 16:53:53 -06'00'	10 June 2019

Approver

Org	Name	Z#	Signature	Approval Date
J-2	Brandy C. Royer	108030	Brandy Royer	6/12/19

Approver

Org	Name	Z#	Signature	Approval Date
ES-55	Ben R. Lopez	092847	BENJAMIN LOPEZ (Affiliate) Digitally signed by BENJAMIN LOPEZ (Affiliate) Date: 2019.06.13 13:38:04 -06'00'	

DOES NOT CONTAIN
UNCLASSIFIED CONTROLLED
NUCLEAR INFORMATION

Reviewing/
Denying
Official: Gene N. Ortega / ES-55
Name and organization

Date: 06/04/19

EXECUTIVE SUMMARY

The Isotope Fuel Impact Tester (IFIT) at PF-4 is a specialized set of equipment designed for simulating high-speed impact of experimental parts. The IFIT is an inert gas launcher designed to impact $^{238}PuO_2$ heat source assemblies, fuel encapsulation materials, structural materials, and subassemblies of radioisotope thermoelectric generators (RTGs). TA-55 management desires to re-use outer catch tube (OCT) of the milli-watt (MW), multi-hundred watt (MHW) and general purpose heat source (GPHS) designs and thus requires a technical evaluation of potential life cycles to failure. This report provides a fitness-for-service (FFS) assessment using fracture mechanics techniques based on the state-of-stress developed with the aid of a computational finite element model (FEM) of the IFIT. Importantly, the report describes the different material options for the OCT; H-11 vacuum-arc re-melted (VAR) and H-13 VAR for a given heat treatment resulting in a Rockwell-C hardness of 42, and an additional option of 4340 alloy steel with a range of heat treatment resulting in Rockwell-C hardness of 40 to 44.

A finite element analysis (FEA) developed by W-13 in 2009, whose purpose was to reveal the deformation state of one-time use components involved in the impact, provides through-thickness stress distribution plots of each design; MW, MHW and GPHS. This data is used as input to a fitness-for-service, fracture mechanics assessment presupposing that a flaw already exists at the worst stressed location. The fracture mechanics assessment provides results in OCT cycles-to-failure, where a cycle is equivalent to a single shot sequence. Two typical flaws are evaluated using the ASME Code, Section VIII, Division 3, recommended starting flaw size: (a) semi-elliptical surface (i.e., thumbnail) flaw of 1/16” deep by 3/16” long and (b) annular surface flaw of 1/16” deep by 360° circumference.

Lastly, three additional conditions have been evaluated herein:

(a) reduced velocity for the 12.7 kg aluminum outer projectile cylinder (OPC) impact that would provide significant number of cycles before component failure,
(b) an increase of OPC mass to 25 kg and determine maximum allowable velocity to support a significant number of cycles before component failure and
(c) change OPC material from aluminum to brass and determine maximum allowable velocity to support a significant number of cycles before component failure.

Results of the evaluation are shown in Tables below. Finally, it should be understood that if, and only if, non-destructive evaluation (NDE) methods determine that the inner and outer surfaces of the OCT are free from surface and subsurface indications (i.e., flaws), or that surface flaws are observed to be smaller than those recommended by the ASME Code, re-use cycles-to-failure of the OCT may be increased for higher impact velocities.

OCT Shot Cycles-to-Failure for Thumbnail Flaw

Velocity, (m/s)	Alum 12.7 kg	Alum 25 kg	Brass 39.4 kg	Brass 77.6 kg
200	FAILURE			
190	87	Failure	Failure	Failure
180	415			
170	879			
160	1732			
150	3193			
140	5923			
138	6580	11		
130	10803	319		
120	Greater than 20K cycles.	985		
110		2428	11	
100		5819	554	
90		13665	1886	
80		Greater than 20K cycles.	5609	
78			6920	23
75			9384	217
70			16465	704
60			51584	3569

OCT Shot Cycles-to-Failure for Annular Flaw (360°)

Velocity, (m/s)	Alum 12.7 kg	Alum 25 kg	Brass 39.4 kg	Brass 77.6 kg
165	11	Failure	Failure	Failure
160	96			
150	369			
140	913			
130	1949			
120	4047			
117	4973	22		
115	5855	70		
110	8282	229		
100	17407	905		
93	Greater than 20K cycles.	---	22	
90		2595	124	
80		7145	848	
70		19837	3201	
66		---	5360	34
60		---	11530	442
50		---	43329	3162
40			198730	18988

Note: Dashes in table cells imply that no calculation was performed.

Table of Contents

Table of Figures

List of Tables

ACRONYMS

ASM	American Society for Metals
ASME	American Society for Mechanical Engineers
FEA	Finite element analysis
FEM	Finite element model
FAD	Failure assessment diagram
FFS	Fitness-for-Service
GPHS	General purpose heat-source
HRC	Rockwell C hardness
ICT	Inner catch-tube
IFIT	Isotope Fuel Impact Tester
IPC	Inner projectile cylinder
MW	Milli-watt
MHW	Multi-hundred Watt
MT	Magnetic particle examination
NDE	Non-destructive examination
NDT	Non-destructive testing
OCT	Outer catch tube
OPC	Outer projectile cylinder
PT	Liquid penetrant examination
RT	Radiographic examination
RTG	Radioisotope thermoelectric generators
UT	Ultrasonic examination
VAR	Vacuum-arc re-melted
VT	Visual examination

1.0 INTRODUCTION

A fitness-for-service (FFS) evaluation of the Isotope Fuel Impact Tester (IFIT) outer catch-tube sub-assembly for the GPHS, MHW and MW design concepts is required to determine its structural integrity for re-use, or in other words, multiple cycles of dynamic load application. State-of-stress data from a transient finite element analysis (FEA) is used as input to the fracture mechanics evaluation, utilizing a Failure Assessment Diagram (FAD) approach, in accordance with API-579.

2.0 BACKGROUND

The IFIT [1] is comprised of a 178mm (7-inch) bore inert-gas launch tube designed to impact a projectile carrying heated samples of $^{238}PuO_2$ heat source assemblies, fuel encapsulation materials, structural materials, and subassemblies of radioisotope thermoelectric generators (RTGs). Figure 1 illustrates the experimental set-up, with the IFIT inner and outer catch-tube components located near the top of this figure. Figure 2 shows a close-up view of the upper portion of IFIT with the inner/outer catch tubes. The outer catch-tube (OCT) effectively stops the 12.7 kg (28 lb) outer projectile cylinder (OPC) mass, which carries the inner projectile cylinder (IPC) traveling up to a maximum of 200 m/s (656 ft/s). OCT subassembly cross-sections for the GPHS, MHW and MW design are shown in Section 2.2 through Section 2.4.

Finally, the experimental set-up can also be modified to accept:

1. OPC mass of 25 kg and
2. brass OPC instead of aluminum.

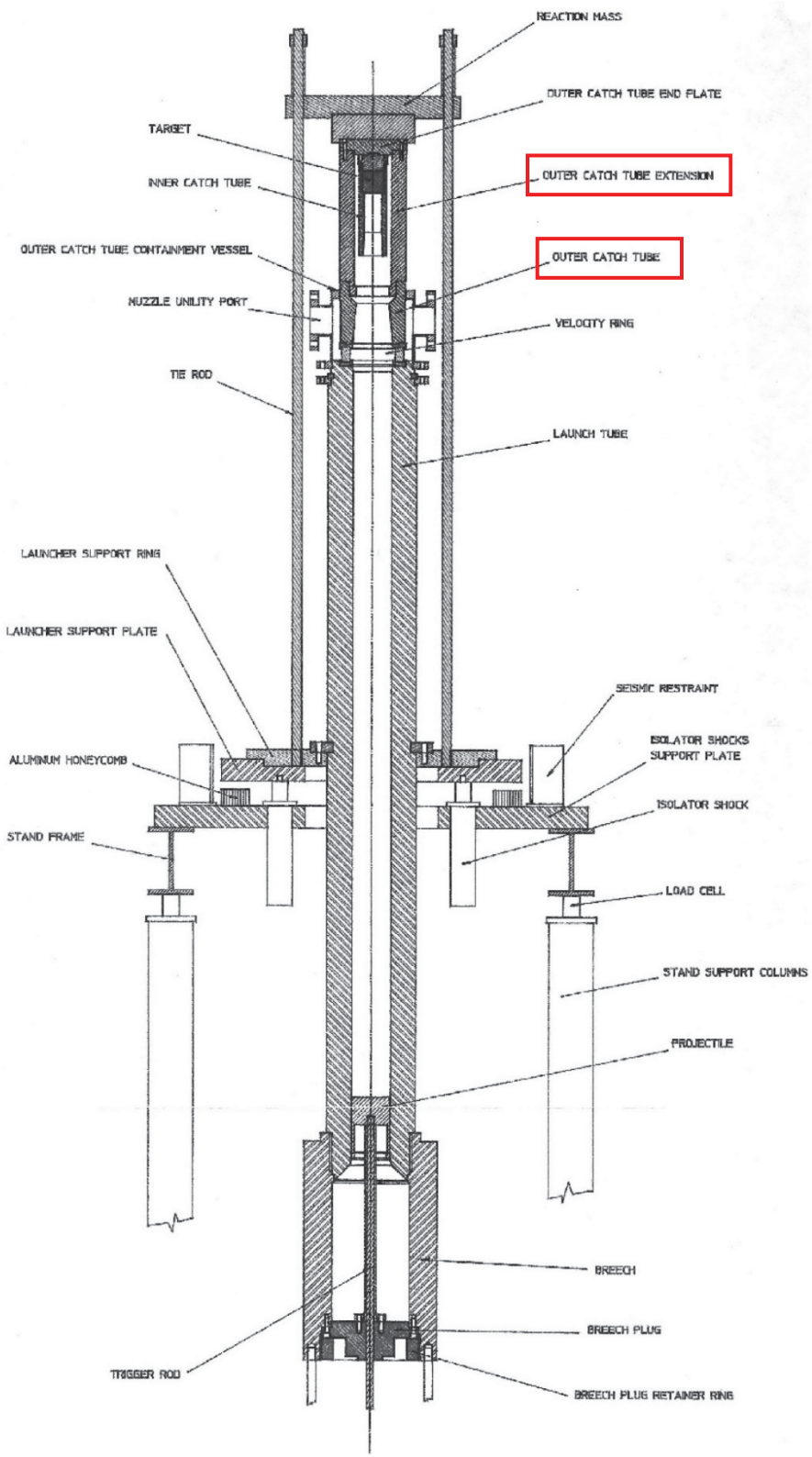

Figure 1 – IFIT and MHW OCT design.

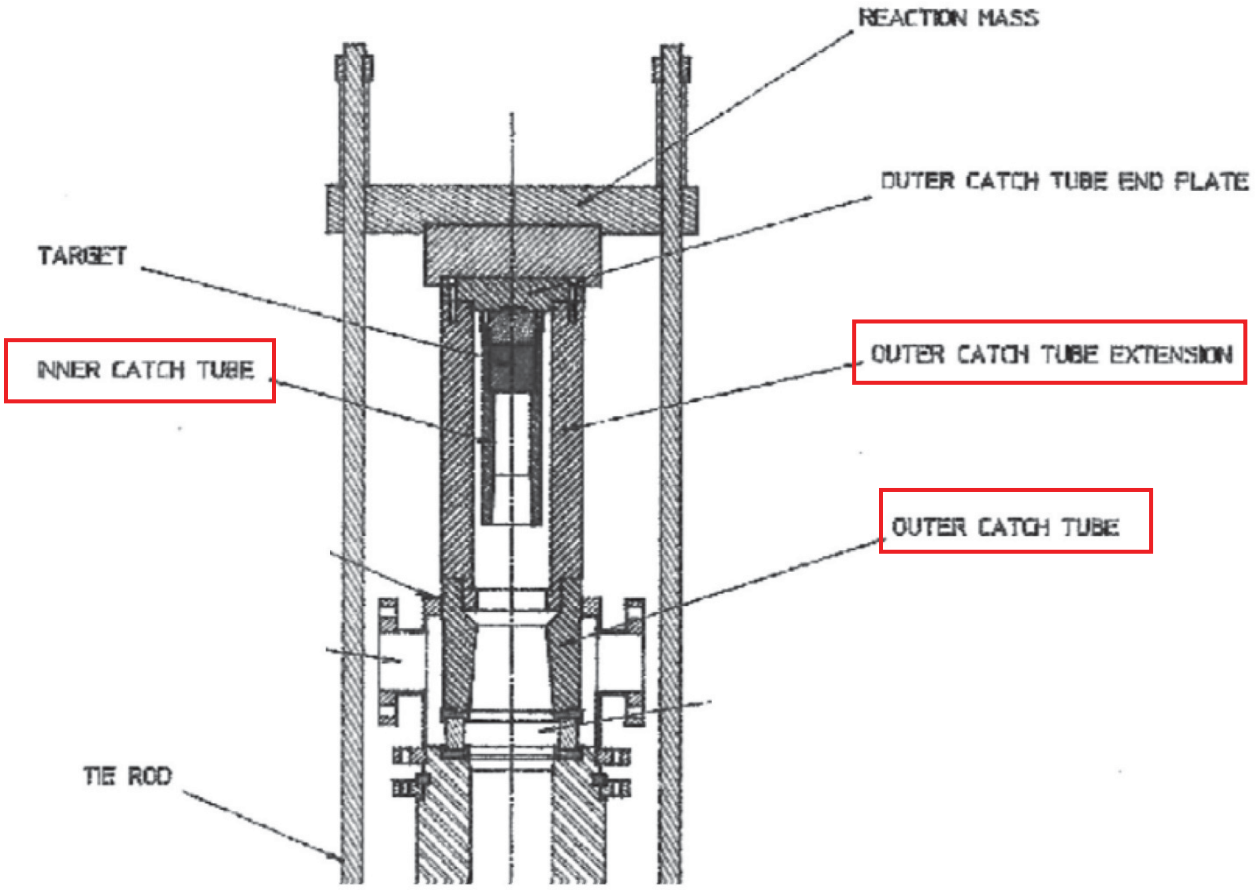

Figure 2 – Upper portion of IFIT with Inner and Outer catch tube subassemblies.

2.1 Computational Models

An explicit FEA model analysis was developed in 2009 by W-13 engineering staff [2], which documented the dynamic state-of-stress from impact conditions of the OCT, and the resulting permanent deformation and plastic strain accumulation of the IFIT assembly. Although the document provides a basis and results of the FE model and analyses, the actual model and raw data for component through-thickness stresses are not available. The only technical information that can be relied upon, with some difficulty, are the color contour plots shown in the W-13 report [2]. Furthermore, because the W-13 report is "a copy of a copy" of the original report, some loss in translation of stress contours is inevitable. A plot of principal stresses is extracted from [2] and shown below as Figure 3.

Unfortunately, the quality of the electronic file and printed document is extremely poor, resulting in color blotches that are difficult to discern, especially through-thickness stress gradients.

Further, the region of the outer catch-tube is highly faded with no particular details of stress concentrations in the notched regions, which in fact exist. However, a straightforward approach that conservatively estimates the state-of-stress will be used herein for the fracture mechanics assessment and is further discussed under Fracture Analysis Method, Section 5.

The W-13 report states that the larger deformation appear to be localized near the impact interface between the outer projectile cylinder and the outer catch tube assembly. Results show von Mises stresses of ~150 ksi on the inner surface, which are considered highly localized, and peak stresses of 170 ksi over a relatively small region, consistent with stress concentrations.

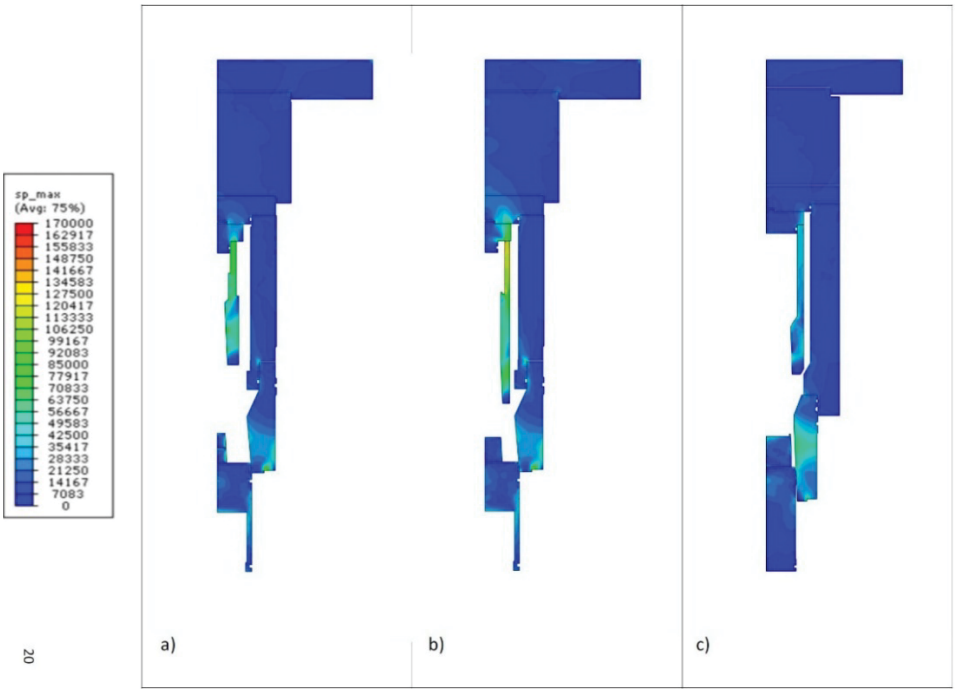

Figure 3 – Principal stresses for a) Milli-watt, b) MHW, and c) GPHS IFIT.

2.2 GPHS OCT Design

The GPHS OCT has a single design with a 2.5° taper (see Figure 5), manufactured from H-13 steel and heat treated to Rockwell C hardness (HRC) of 40 to 44. The current drawing also shows alternate materials such as H-11 heat treated to HRC 40 to 44, and 4340 alloy steel heat treated to HRC of 35 to 40. However, LANL management has requested inclusion of 4340 alloy steel, with heat treatment to HRC of 40 to 44, because this material is readily accessible, where H-11 VAR and H-13 VAR are not currently accessible. Through-thickness stress distribution in the OCT (as shown in Figure 5) depicts an inner diameter maximum principal stress of ~70 ksi reducing to 25 ksi at the outer diameter. The distribution for the GPHS (Figure 5) can be decomposed into 47.5 ksi bending stress and 22.5 ksi membrane stress, which is less severe than the MHW OCT design.

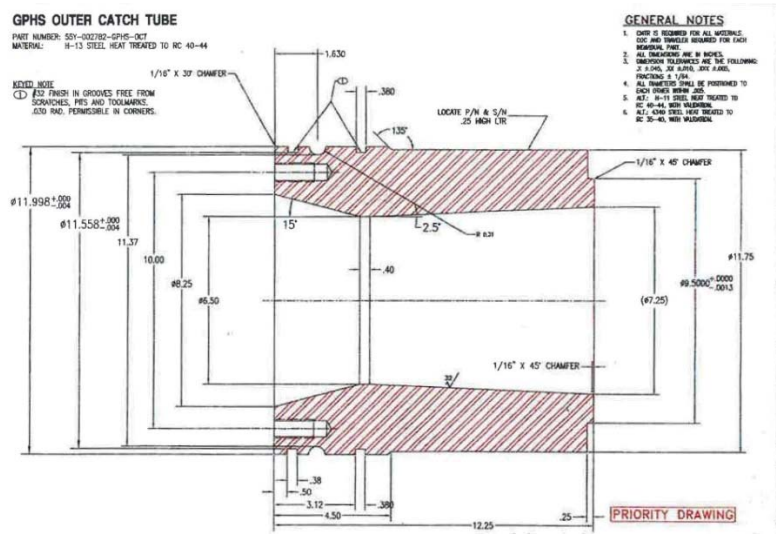

Figure 4 – Outer catch-tube; 2.5° GPHS design.

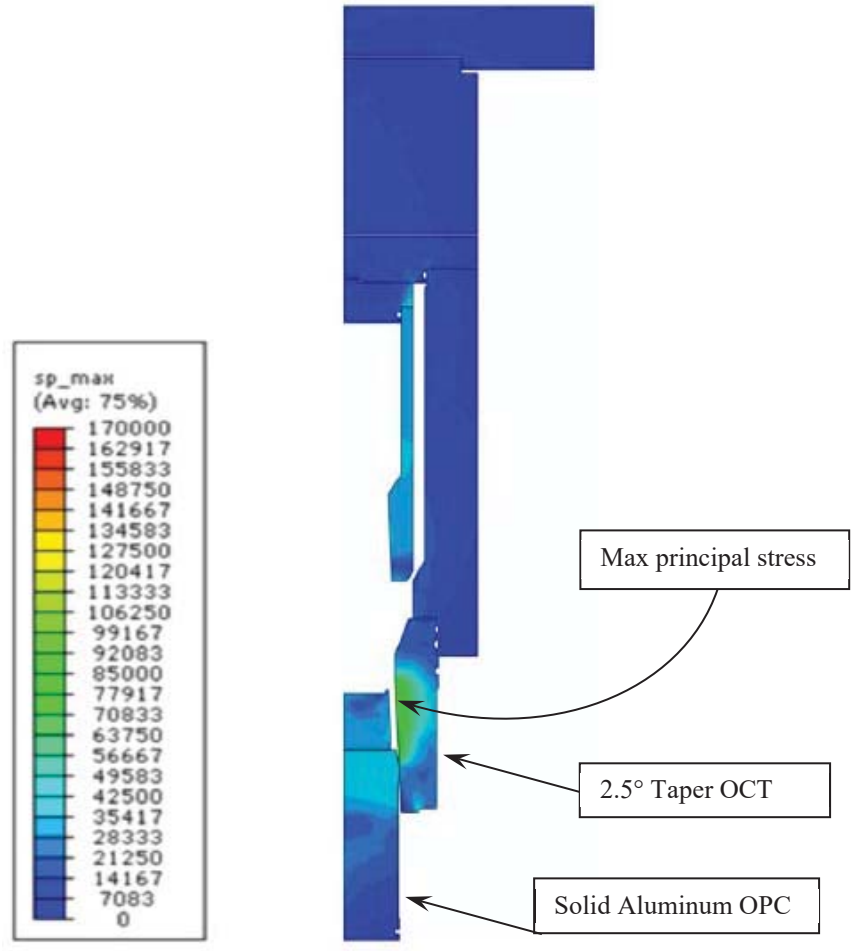

Figure 5 – Principal stresses for GPHS IFIT design.

2.3 MHW OCT Design

The MHW design has three different OCT's of 5°, 4° and 2.5° taper, as shown in Figure 6, Figure 7 and Figure 8, respectively. Currently, the design calls for H-13 vacuum arc re-melted (VAR) steel, heat treated to HRC of 42, and an alternate material H-11 VAR, likewise heat treated to HRC of 42. As previously stated, LANL management has requested inclusion of another alternate material, 4340 alloy steel, for all three OCT tapers, with heat treatment to HRC of 40 to 44.

Table 1 – MHW OCT's Materials

OCT	Material	HRC	Notes
5° Taper	H-13 VAR H11 VAR **4340 Alloy**	42 42 **40-44**	Current allowed materials per LANL drawing are H-11 and H-13. Modify drawing to allow 4340 alloy as shown in bold.
4° Taper	4340 Alloy **4340 Alloy**	36-38 **40-44**	Current allowed materials per LANL drawing is 4340 alloy in heat treatment with HRC 36-38. Modify drawing to suit 4340 alloy with HRC 40-44.
2.5° Taper	4340 Alloy **4340 Alloy**	36-38 **40-44**	

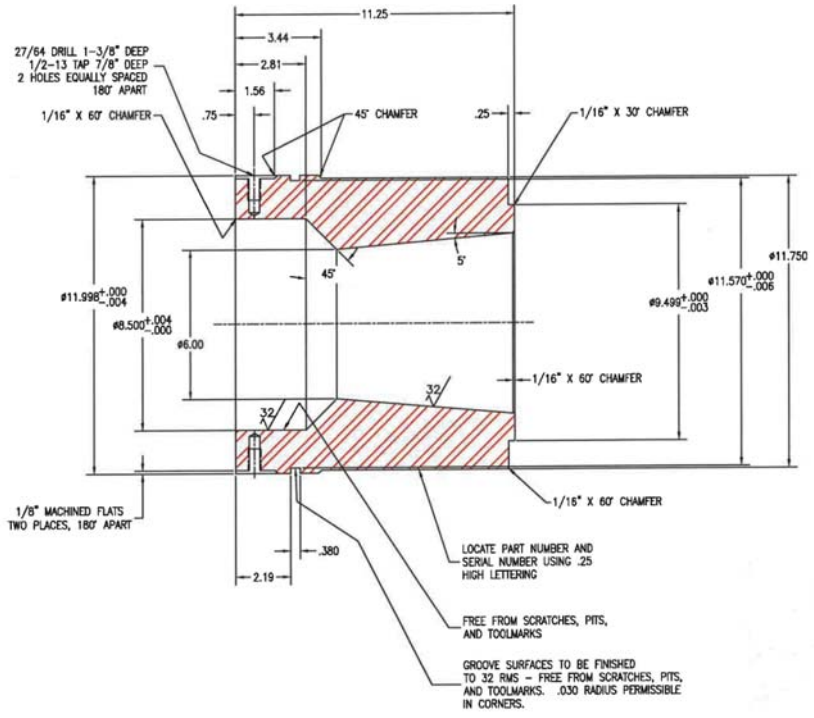

Figure 6 – Outer catch-tube; 5° MHW design.

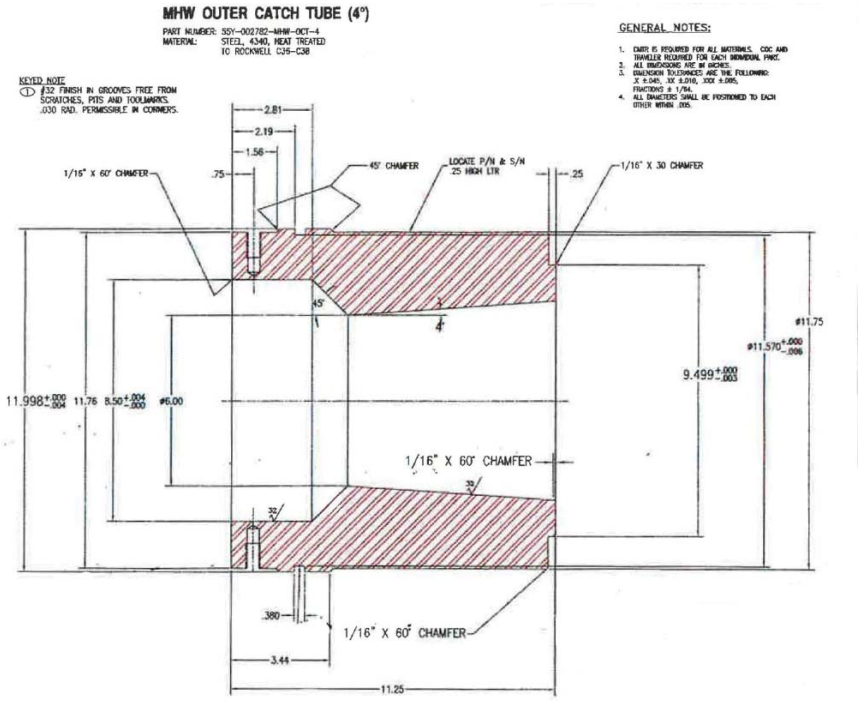

Figure 7 – Outer catch-tube; 4° MHW design.

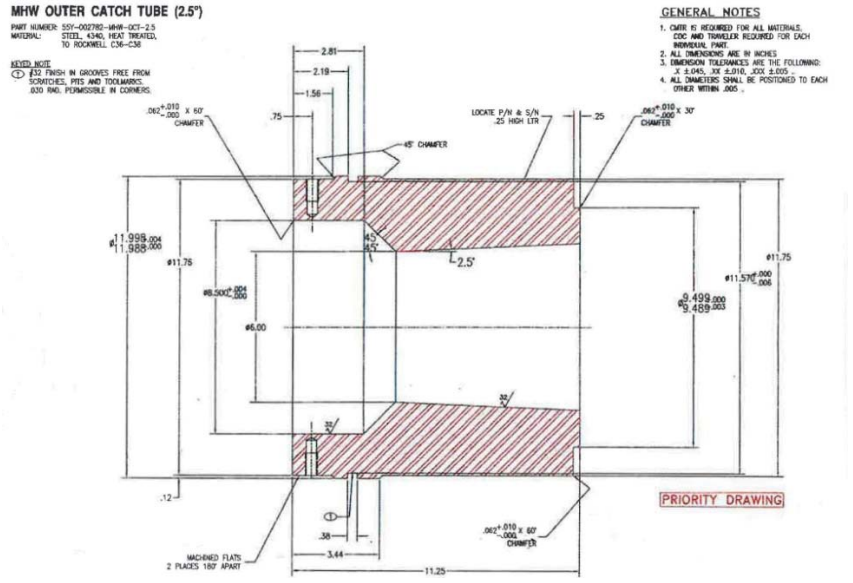

Figure 8 – Outer catch-tube; 2.5° MHW design.

A closer zoom image of the MHW design principal stress plot, listed as Figure 9, shows a light-blue-to-light-green color contour in the vicinity of 70-60 ksi stress for the OCT, with a peak possibly around 150 ksi at the notched corner (i.e., stress concentration). The inner catch tube (ICT) is much more highly stressed than the OCT. Assuming a full through-thickness membrane stress of 70 ksi in the OCT would be rather conservative.

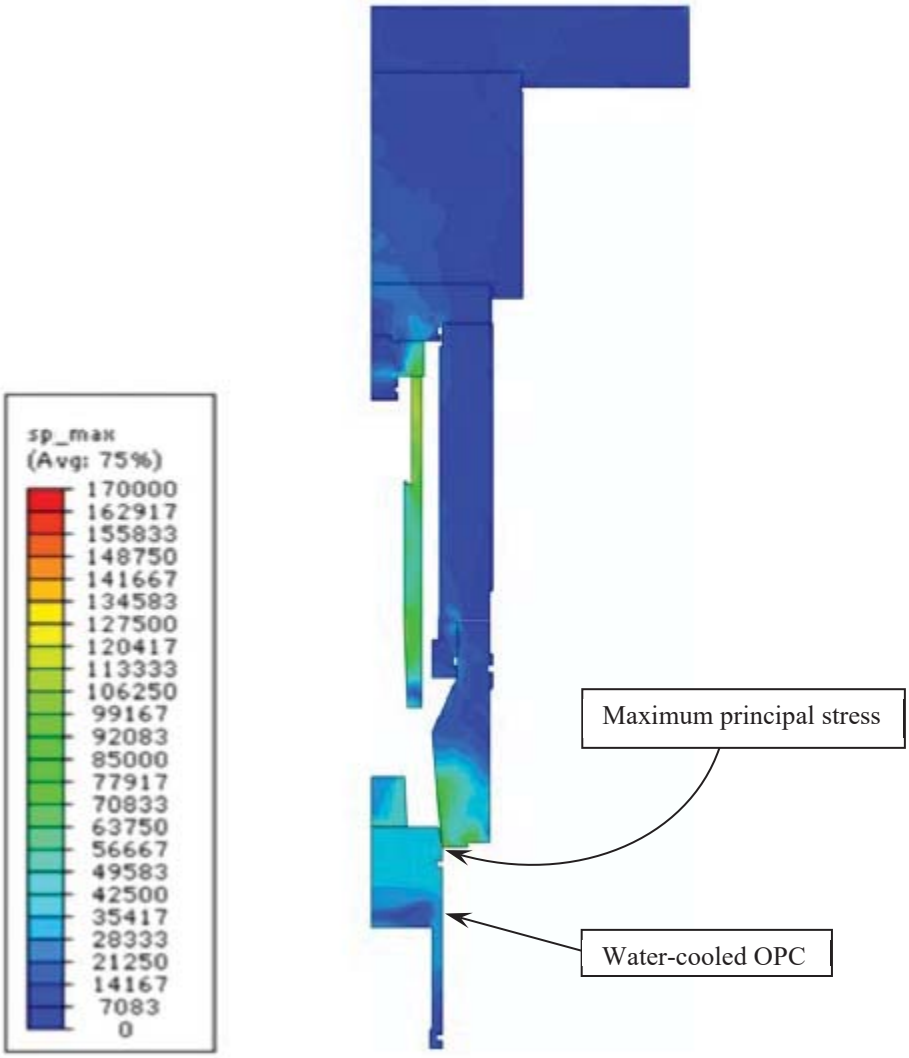

Figure 9 – Principal stresses for MHW IFIT design.

2.3.1 Stress Components for MHW Tapered OCT

The MHW design incorporates three separate OCT's with different tapers of 5°, 4° and 2.5°. However, the W-13 report only focused upon, and provided stresses for, the MHW design with a 5° taper. As such, it is imperative to understand which taper design, subjected to an impact loading, would be the highest stressed. Herein, a simplified methodology is presented to address this issue.

Each OCT has a slight taper to arrest the impact from the outer projectile cylinder, thus allowing the inner projectile cylinder (IPC) and specimen sample mass atop to continue travelling towards the inner catch tube (ICT). Aside from the taper angle, each OCT is identical in dimensions; outer dimeter, inner diameter, etc. However, the OCT opening diameter at the tapered-end is the largest for the 5° taper and is the smallest opening diameter for the 2.5° taper. As shown in Figure 10, both normal (F_N) and tangential (F_T) forces are developed from the impacting force (F_I) from outer projectile cylinder (OPC) onto the tapered OCT.

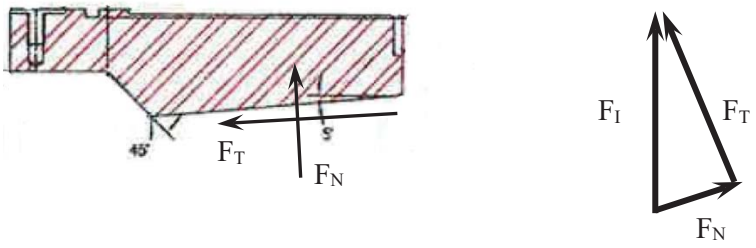

Figure 10 – Normal and tangential forces on OCT taper.

The normal force on the taper section tends to radially expand the OCT cylinder, producing very large hoop stresses. Decomposing the normal and tangential forces shows that for a given impact kinetic energy, the normal force will be a function of the sine of the taper angle (i.e., sin θ) and the tangential force a function of the cosine (i.e., cos θ). Normal and tangential force components for each taper design is listed in Table 2.

Table 2 – Normal and Tangential Force Components

OCT Taper	Normal	Tangential
5	0.0872	0.996
4	0.0698	0.998
2.5	0.0436	0.999

The above table shows that although the tangential force component is practically the same for all three OCT tapers, the normal force component for the 5° taper is twice the magnitude of the

2.5° taper. This implies that the 5° taper OCT design will result in higher stresses, and therefore the W-13 report does list the maximum stresses for any of the three MHW OCT taper designs.

2.4 MW OCT Design

The milli-watt design uses interchangeable OCT's from the GPHS and MHW. As such, the 5°, 4° and 2.5° taper OCT's shown in Section 2.2 and 2.3 may be appropriated by the MW design. This design also shows that OCT stresses are somewhat lower than the inner catch tube (ICT) stresses by almost a factor of two. Principal stresses in OCT are comparable to MHW OCT as shown in Figure 9.

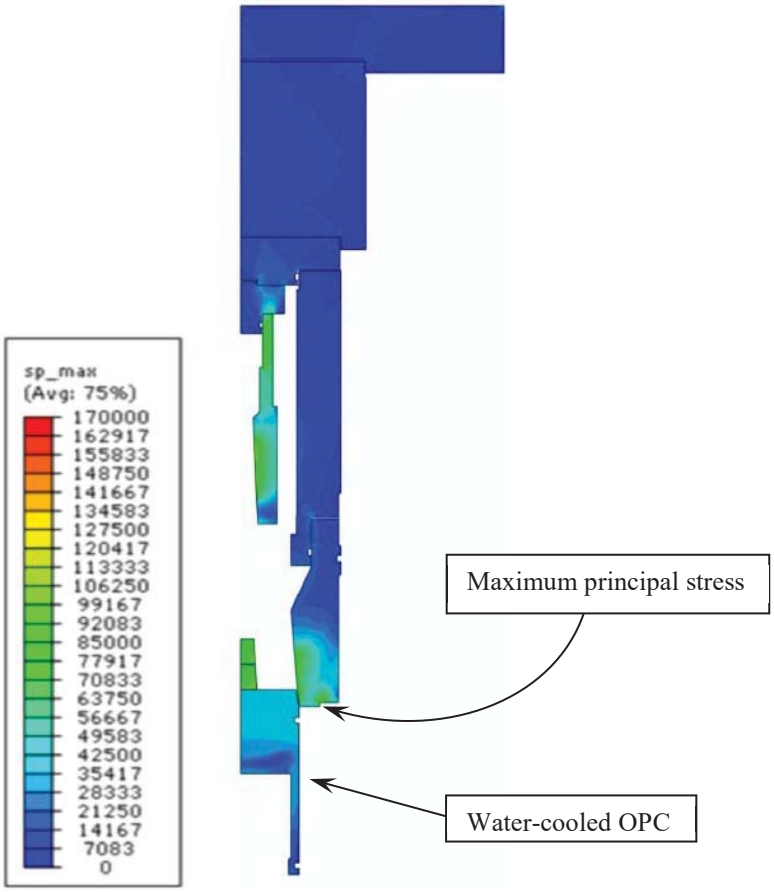

Figure 11 – Principal stresses for MW IFIT design.

3.0 MATERIAL PROPERTIES

The original stress analysis by W-13 staff [2] was conducted using physical and mechanical properties consistent with ultra-high-strength steels, H-11 or H-13 for the outer catch-tube, and 4340 steel for the outer catch-tube extension. LANL intends on further modifying the IFIT drawings to allow use of 4340 alloy steel for the OCT, with heat treatment within the range of

Rockwell-C hardness of 40 to 44. Chemistry for H-11, H-13 and 4340 steels are listed in Table 3 and Table 4.

No Certified Material Test Report (CMTR) data was provided for the MW, MHW or GPHS IFIT outer catch tube sub-assembly. However, TA-55 staff, Art Herrera [3], attests to a total of 390 shots performed on 3 separate outer catch-tube components (i.e., 2.5°, 4° and 5° taper design) manufactured from vacuum-arc-re-melted (VAR) H-11, H-13 and 4340. Thus, we make the implicit assumption herein that each separate taper design has been fired at least 130 times (or possibly more).

Minimum specified material properties will be utilized in these calculations, along with fracture toughness (K_{Ic}) and Charpy V-notch (CVN) impact properties obtained from Center for Information and Numerical Data Analysis and Synthesis (CINDAS) Aerospace Structural Metals Handbook [4]. Per LANL drawings, material requirements for Rockwell-C hardness (HRC) notes a value of 42 for H-11 and H-13 and HRC of 40 to 44 for 4340 steel. Using the Rockwell-C hardness-to-ultimate-strength conversion in Appendix A, H-11 VAR, H-13 VAR and 4340 ultimate strength must be around 191 ksi, for HRC of 42. However, as stated previously, LANL intends on modifying the OCT drawing to allow use of 4340 alloy steel, with heat treatment within the range of HRC 40 to 44.

Typical yield strengths of 4340 high-strength alloy steel, along with other high-strength alloys of yield strengths within the range of 130 to 190 ksi, have been correlated by Benet Labs [6] to Rockwell-C hardness. The correlation is shown in Figure 12 and explicitly as:

$$S_y = 4.226HRC$$

Table 3 – Chemical Composition H-11 and H-13 Steel [4,5]

Grade	Carbon	Chrome	Molybdenum	Vanadium
H-11	0.35 – 0.45	4.75 – 5.50	1.10 – 1.60	0.30 – 0.60
H-13	0.32 – 0.45	4.75 – 5.50	1.10 – 1.75	0.80 – 1.20

Table 4 – Chemical Composition 4340 Steel [5]

Grade	Carbon	Nickel	Chrome	Manganese	Molybdenum
4340	0.37 – 0.44	1.55 – 2.00	0.65 – 0.95	0.55 – 0.90	0.20 – 0.35

The engineering mechanical properties for all steels are obtained from CINDAS [4] and the ASM Handbook [5].

Table 5 – Mechanical Properties [4,5]

Grade	HRC	Sy (ksi)	Su (ksi)	E (ksi)	%Elong.	%RA	CVN (ft-lb)
H-11 H-13	42	160	191	29E+3	14	38	9(1)
4340(2-4)	40	169(4)	182		13(2,3)	50(2,3)	14(2,3)
	41	173	187		12	48	
	42	177.5	191		11	47	
	43	182	196		10.5	46	
	44	186	200		10	45	

(1) See Appendix B
(2) See Appendix C
(3) See Reference [5]
(4) See Reference [6].

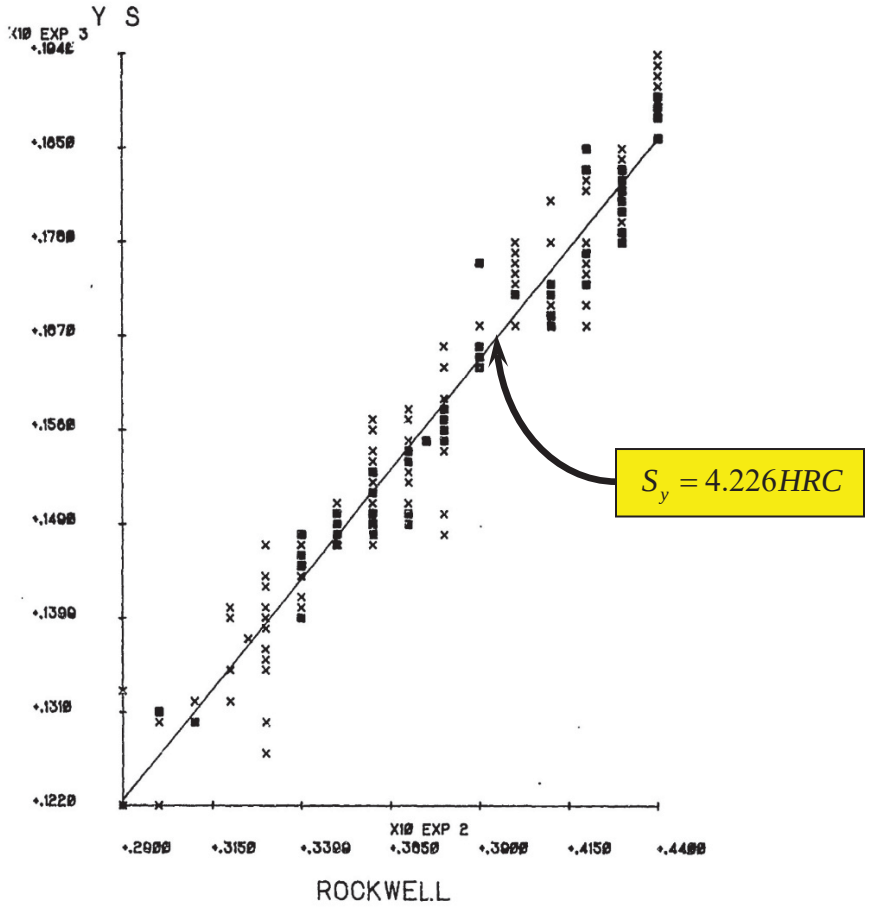

Figure 12 – Yield Strength to Rockwell-C Hardness Correlation [6].

True stress-strain curve for H-11 and H-13 are practically identical, since the material properties (see Table 5) are equivalent. Likewise, although 4340 has a slightly higher proportional limit, the true stress-strain curve is similar to H-11 and H-13 steel (see Figure 13) for HRC of 42. Heat treatment of 4340 steel to HRC of 40-44 definitely show a significant difference in true-stress, true-strain behavior. These data utilize a constitutive material model utilizing a power-law approximation as described by Rodriguez [7]. Power-law parameters are itemized in Table 6, and represented by the true-stress, σ, as a function of true-strain, ε.

$$\sigma = \sigma_o \varepsilon^n$$

H-11 & H-13 Steel	4340 Alloy Steel
HRC=42	HRC = 42
$\sigma = 268.18\varepsilon^{0.104}$	$\sigma = 241.76\varepsilon^{0.0625}$

Table 6 – True Stress-Strain Parameters

Grade	HRC	σ_o	n	ε_{PL}	σ_{PL}	ε_{Ult}	σ_{Ult}	ε_{Fail}	σ_{Fail}
H-11 & H-13	42	268.18	0.104	0.00537	155.72	0.104	211.93	0.478	248.37
4340	40	230.00	0.0619	0.00576	167.17	0.0619	193.62	0.6932	224.84
	41	237.79	0.0641	0.00590	171.10	0.0641	199.39	0.6539	231.40
	42	241.76	0.0625	0.00606	175.74	0.0625	203.31	0.6349	235.00
	43	248.71	0.0634	0.00622	180.26	0.0634	208.82	0.6162	241.19
	44	253.56	0.0631	0.00636	184.33	0.0631	213.02	0.5978	245.47

Nomenclature:

σ_o = Power-law coefficient

n = Power-law exponent

ε_{PL} = True strain at proportional limit

σ_{PL} = True stress at proportional limit

ε_{Ult} = True ultimate strain

σ_{Ult} = True ultimate stress

ε_{Fail} = True strain at failure

σ_{Fail} = True stress at failure

The true strain at failure is governed by the reduction of area (%RA) of the material. As evident with 4340 steel at about 205 – 210 ksi, the true ultimate strength is comparable in both H-11 and H-13, and 4340 is slightly higher. Power-law relationship comparison of typical minimum specified mechanical properties is shown in Figure 13.

Based on the material failure stress (σ_{Fail}) shown in Table 6 for H-11, H-13 and 4340 alloy steel, the contour stresses in Figure 9 within the light-blue-to-light-green color-band, range between 65 – 70 ksi, which are considered stresses in the linear elastic region because they are well below the 230 – 240 ksi failure limit and well-below the proportional limit of 155 – 175 ksi. The maximum principal stress at the notched corner (see Figure 9) appears to be around 120 ksi, which again would be below the elastic limit of the material. In fact, stresses appear to be at or near half-yield throughout a large section of the component. As such, the bulk of the MHW OCT assembly may be considered as responding in a purely linear-elastic fashion.

Although a ductile failure is not predicted, it is nevertheless necessary to determine whether a surface flaw subjected to repeated cycling of loads could cause a critical crack to run unstably.

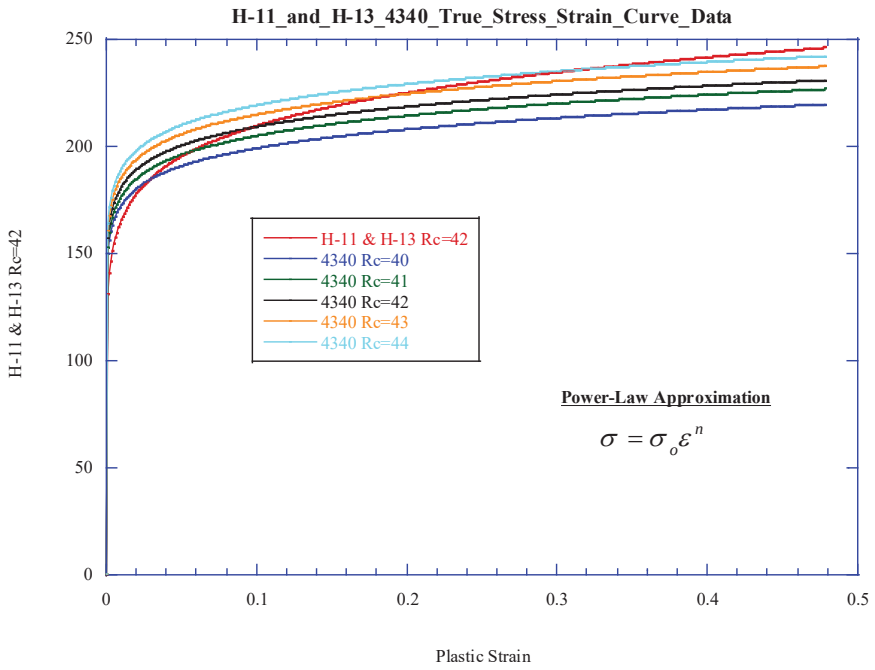

Figure 13 – True stress-strain curve for H-11, H-13 and 4340 steel IFIT material.

4.0 JUSTIFICATION OF IMPULSIVE EVENT

ASME Code Case 2564 [8] was developed to address design and analysis of structures for impulsive loadings as part of ASME Code, Sec. VIII, Div. 3 [9], where the pulse duration is only a fraction of the structural period of vibration. The code case stipulates that an event is considered impulsive when the pressure-pulse duration is 35%, or below, of the fundamental membrane dominated structural-period of vibration. For the MHW OCT sub-assembly, the impact event is treated from an impulse-momentum principle, idealizing the impulse as a triangular function, such that:

$$\int F dt = mv$$

where $F =$ Axial force acting on tube, (lb)

$m = \dfrac{W}{g}$

$W =$ Weight of projectile

$g =$ Gravitational constant (386.4 in/sec^2)

$m =$ Projectile mass, (lb-sec^2/in)

$v =$ Projectile velocity, (in/sec)

Projectile weight is 12.7 kg or 28 lb, resulting in momentum of:

$$mv = \left(\frac{28\ lb}{386.4\ in/s^2}\right)\left(656.17\ ft/s\right)\left(12\ in/\ ft\right)$$

$$mv = 570\ lb - s$$

To obtain the axial force acting on the tube, we estimate using the average stress from Figure 9, taken here as 70 ksi, over the minimum cross-sectional area from Figure 6:

$F = \sigma A$

$\sigma =$ Average axial stress, (ksi)

$A =$ Cross-sectional area, (in^2)

$A = \dfrac{\pi}{4}\left(D_o^2 - D_i^2\right)$ $\quad D_o = 11.75$ in $\quad D_i = 8.50$ in

The calculated axial force is:

$$F = 3618 \text{ kip}$$

The resulting pulse period is representative of a triangular-pulse shape, consistent with an immediate load which decays rapidly.

$$\Delta t = \frac{2mv}{F} \qquad \Delta t = 0.315 \text{ ms}$$

Fundamental membrane dominated axial tube frequency as described by Blevins [10] is governed by:

$$f = \frac{1}{2\pi}\left[\frac{k}{m}\right]^{1/2}$$

and $$k = \frac{AE}{L} \qquad m = \frac{W}{g} \qquad f = \frac{1}{2\pi}\left[\frac{AEg}{WL}\right]^{1/2}$$

where
$L =$ Length of tube, (in)
$L = 20$ in (i.e., includes outer catch-tube extension)
$E =$ Modulus of elasticity, (lb/in^2)
$E =$ 29E+6
$g =$ Gravitational constant, (in/sec^2)
$g = 386.4$
$\rho =$ Density of tube, (lb/in^3)
$\rho = 0.2835$

Resulting frequency, f, and period-of-vibration, T, are:

$$f = 5118.5 \text{ Hz} \qquad T = 0.195 \text{ ms}$$

Therefore, $\frac{\Delta t}{T} = \frac{0.315 \text{ ms}}{0.195 \text{ ms}} = 1.60$ (Does not meet Code Case 2564 criteria of ≤ 0.35).

Because Code Case 2564 criteria is not met for the IFIT OCT, the implication is that stresses developed during the dynamic event are not within the impulsive regime (i.e., at $\Delta t/T \leq 0.35$) as shown in Figure 14, yet are definitely within the mixed-mode dynamic regime, and therefore stresses are considered "primary" (i.e., load controlled). As a consequence, equipment could be subject to catastrophic failure from a ductile rupture generally caused by "primary" stresses.

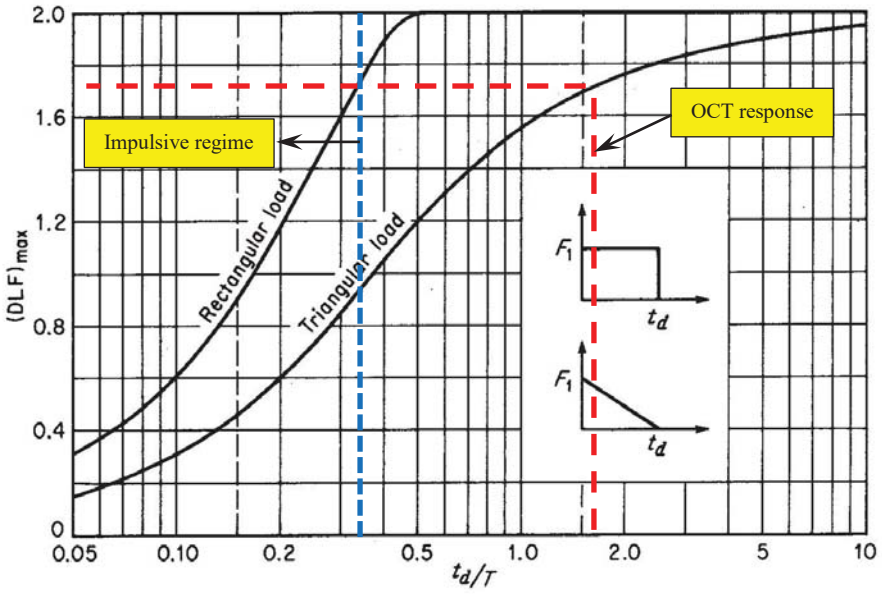

Figure 14 – Dynamic load factors for SDOF structural response [11].

The implication of the above conclusion is that for the fracture mechanics analyses in Section 5 through Section 8, all far-field stresses away from a crack-tip must be considered primary in lieu of secondary.

5.0 FRACTURE MECHANICS ANALYSIS METHOD

The propensity for brittle fracture of a component is dependent on the size and geometry of a surface flaw or embedded flaw, applied stress, and material's resistance to fracture, i.e., notch or fracture toughness, CVN or K_{Ic}, respectively.

As mentioned earlier, there are no detailed data available for the stress analysis results presented in the W-13 document [2]. Additionally, W-13 has not been able to locate any of the electronic input or output files for the FEA model, which would alleviate the potential to develop a new model, if absolutely necessary. Thus, an alternative approach to that requiring actual through-thickness stress gradients will be used herein.

The fracture mechanics analysis procedure follows rules in the ASME B&PV Code, Sec. VIII, Div. 3 [9], Code Case 2564 for Impulsively Loaded Vessels [8] and guidance contained in API-579/ASME FFS-1 [12] for calculating stress intensity factors at the crack-tip. Additionally, the Failure Assessment Diagram (FAD) approach, per API-579/ASME-FFS [12], is followed herein that addresses the interaction between brittle fracture and ductile failure.

5.1 Stress Classification and FAD

An important consideration for whether a brittle fracture could occur under a given stress-field is understanding the type, and classification, of applied stresses on the component. That is, using ASME Code definition of *"primary stress"* for a load-controlled situation versus *"secondary stress"* for a displacement-controlled event, the fracture mechanics analysis considers each of these stresses, and therefore each stress intensity factor, K_I^P and K_I^{SR}.

where K_I^P = Stress intensity factor for primary stress, (ksi-in$^{1/2}$)

K_I^{SR} = Stress intensity factor for secondary and residual stress, (ksi-in$^{1/2}$)

The total stress intensity factor at the crack-tip is described in API-579/ASME-FFS [12] and shown below.

Uniform external or internal loads, such as constant internal pressure, would result in "primary" stresses on the component, which would be limited by the ductility measures such as yield strength and percent elongation. Under time-dependent loading within the impulsive regime, where the pulse-period is much shorter than the structural-period of the component $\Delta t/T \leq 0.35$, stresses generated are considered purely "secondary" [12,13]. The FAD approach is a graphical tool representing an interaction between the toughness-ratio, K_r, and primary load-ratio, L_r^P, as described by**:**

$$K_r = \left[1 - 0.14\left(L_r^P\right)^2\right]\left\{0.3 + 0.7\exp\left[0.65\left(L_r^P\right)^6\right]\right\}$$

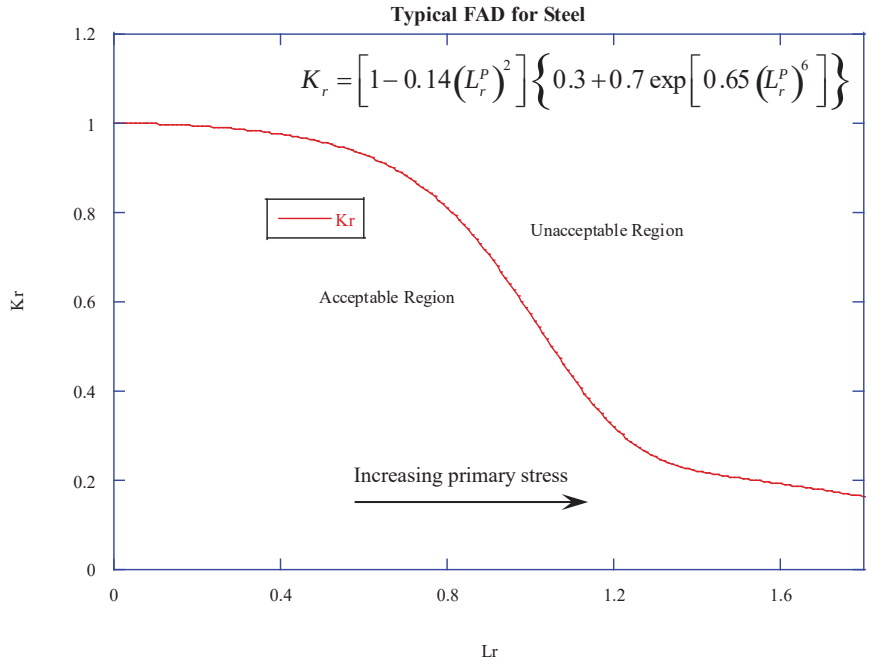

Figure 15 – FAD for ductile materials.

where $K_r = \dfrac{K_I^P + \Phi K_I^{SR}}{K_{mat}}$

$L_r^P = \dfrac{\sigma_{ref}^P}{\sigma_{ys}}$

Φ = Plasticity interaction factor

K_I^P = Crack-tip stress intensity factor for primary stresses

K_I^{SR} = Crack-tip stress intensity factor for secondary and residual stresses

K_{mat} = Material fracture toughness or K_{Ic}

K_{Ic} = Plane-strain fracture toughness of material

σ_{ref}^P = Reference stress for the given geometry structure

σ_{ys} = Engineering yield strength of material

For impact or impulsive events with no initial, or long-term, "primary" stress loading, the L_r^P ratio is considered null (i.e., zero). The implication is that a flawed component can withstand a much larger stress, or flaw size, because it doesn't compete with effects of ductile failure. In other words, the concern here is addressing the fracture ratio, K_r, for $L_r^P = 0$ (see Figure 15).

For a complete review and additional insight of the philosophy presented above, please refer to W-14 staff report by Rodriguez [13], Section 9.3. Additionally, the Journal of Pressure Vessel Technology article by T. Duffey [14] describes the instability mechanisms not present for impulsive loadings, that being "primary" stresses.

5.2 Applied Stress

Using details of the colored stress-contours in Figure 9, an estimate of the maximum principal stress anywhere in the component is obtained for the outer catch tube sub-assembly. Furthermore, this maximum principal stress is assumed to be uniform through-thickness, i.e., no stress gradient, thus conservatively upper-bounding the stress intensity factor (K_I) at the crack-tip for a given flaw geometry. Although employing a more complex form in the analysis, this is simply described here as a function of flaw geometry, C, stress, σ, and crack depth, a. Therefore, a higher stress will result in a higher stress intensity factor.

$$K_I = f\left(C\sigma\sqrt{\pi a}\right)$$

Based on reviewing several sections of all three component shown in Figure 5, Figure 9 and Figure 11, the maximum uniform through-thickness stress used in the analysis is conservatively:

$$\sigma_{\max} = 70\ ksi$$

This appears to be the maximum stress anywhere among all three OCT components.

5.3 CVN and K_{Ic} Data

Plane-strain fracture toughness data (K_{Ic}) and Charpy V-Notch (CVN) impact data may be employed; which is readily evaluated as an upper-shelf K_{Ic} via the Rolfe-Novak-Barsom correlation [15], if and only if, the CVN resides on the upper-shelf.

$$\left(\frac{K_{mat}}{\sigma_{ys}}\right)^2 = 5\left(\frac{CVN}{\sigma_{ys}} - 0.05\right)$$

where $K_{mat} = K_{Ic} =$ Material fracture toughness, (ksi-in$^{1/2}$)

$\sigma_{ys} =$ Static yield strength, (ksi)

$CVN =$ Charpy V-Notch impact, (ft-lb)

Furthermore, for ultrahigh strength steels such as H-11 and H-13, Leskovšek [16] developed a different conversion, which has been calibrated to CVN and HRC (i.e., Rockwell-C hardness):

$$K_{Ic} = 4.53\left(CVN\right)^{1.1}\left(HRC\right)^{-0.135}$$

Results of the Rolfe-Novak-Barsom and Leskovšek correlations are shown in Table 7, along with CINDAS (K_{Ic}) data from Appendix B for a required HRC = 40-44 for 4340 steel and HRC=42 for H-11 and H-13. It is evident from Table 7 that 4340 steel has a higher fracture toughness than either H-11 and H-13, which is based on CVN data from ASM and CINDAS. Although typical textbook values of CVN are included herein, it is imperative that LANL obtain CMTRs for 4340 alloy and confirm that these values are higher than H-11 and H13 steels.

Table 7 – Fracture Toughness K_{Ic}

Material		CVN (ft-lb)	K_{Ic} (ksi-in$^{1/2}$)		
			Rolfe-Novak-Barsom	Leskovšek	CINDAS
H-11 & H-13		9	28.3	30.7	24
4340	R_c=40	14	68.8	50.2	NA
	R_c=41			50.0	
	R_c=42			49.9	
	R_c=43			49.7	
	R_c=44			49.5	

5.4 Minimum Flaw Size

ASME Code Sec. VIII, Div. 3 [9], Part KE-233.2, specifies requirements for inspectable flaw size under UT and RT inspection criteria. That is, for a component that receives a UT inspection, the minimum flaw size is 3/16" long by 1/3*(3/16") deep (i.e., 1/16" deep) for material thicknesses greater than 2-inch. The outer catch tube sub-assembly is manufactured as 11.75-inch OD by 6-inch ID at the thickest portion, thus a 3/16-inch long flaw by 1/16-inch deep is appropriate. Using the nomenclature from API-579/ASME-FFS [12], the following parameters are used in the calculations herein:

$a = 0.0625"$ (flaw depth)

$2c = 0.1875"$ (flaw length)

5.5 Stress Intensity Factor

Stress intensity factors for cylindrical geometries (i.e., tubes and pipes) are used in this calculation, presuming a surface flaw driven by "primary" axial stresses resulting from the impact. Solutions are itemized in Annex 9B of API-579/ASME-FFS [12] for a cylindrical geometry; Case 9B.5.13 – *"Cylinder – Surface Crack, Circumferential Direction – Semi-Elliptical Shape, Internal Pressure and Net-Section Axial Force."*

$$K_I = G_o \left(\frac{pR_o^2}{R_o^2 - R_i^2} + \frac{F}{\pi\left(R_o^2 - R_i^2\right)} \right) \sqrt{\frac{\pi a}{Q}}$$

where G_o = Influence coefficients (see Pg. 9B-23 in [12])

Q = Crack geometry coefficient

where $Q = 1.0 + 1.464\left(\frac{a}{c}\right)^{1.65}$ *for* $a/c \le 1.0$

Because there is no internal pressure, the first term within the brackets in the above equation is null (i.e., zero). The second term within the brackets is an axial force, F, over the tube cross-section, which herein we specify as the given uniform stress across the thickness (see Section 5.2) developed as a "primary" stress.

A simple crack-growth power-law with the following parameters taken from ASME VIII-3, Article KD-430 is used throughout the fracture mechanics analyses:

$$\frac{da}{dN} = C\left(\Delta K\right)^m$$

where $C = 1.95E-10$

$m = 3.26$

For ease of computations, the Quest Integrity software program SIGNAL-FFS [17] is employed, which contains the complete library of influence coefficients from API-579/ASME-FFS [12].

6.0 ANALYSIS RESULTS

Figure 16 and Figure 17 show the two fatigue-crack-growth (FCG) cases addressed in this analysis

(a) semi-elliptical thumbnail flaw and

(b) full 360° circumferential annular flaw.

Using the lower-bound value of $K_{Ic} = 24\ ksi - in^{1/2}$ for H-11 and H-13 steel per Table 7 and the typical yield strength from Table 5, both cases for the thumbnail flaw and annular flaw result in immediate failure of the component at the maximum conditions. That is, for the given plane-strain fracture toughness and initial flaw size presumed from ASME B&PV Code guidance, the components fail by brittle fracture upon a single application of the impact loading (i.e., 12.7 kg projectile propagating at 200 m/s). It is evident from Table 7 that 4340 steel has a factor of 2 higher fracture toughness than H-11 and H-13, as such, the 4340 steel will not be assessed for crack-growth failure as it would result in much higher number of cycles before failure.

It is evident that since, presumably, there have been over 130 individual shots of each separate outer catch-tube design, the fracture toughness of the actual material must be greater than this lower-bound value. Likewise, there might have been approximately 390 shots of a single outer catch-tube design, which would provide an upper-bound. Alternatively, the 390 prior shot executions could have been performed at lower projectile velocities than the maximum 200 m/s used in the structural analysis by W-13 (D. Crane), thereby accommodating additional crack-growth.

Furthermore, no information has been made available relative to the number of full-amplitude vibration cycles per individual impact shot, as the W-13 analysis did not provide this information. Therefore, herein the assumption is that the system exhibits approximately 10 full-amplitude stress cycles per impact shot before decaying to zero stress. The implication is that for any given impact, the outer catch-tube's dynamic structural response exhibits 10 cycles of full membrane stress per shot, from compression to tension. Thus, the fatigue crack growth calculations consider these additional cycles to overall failure. Figure 18 and Figure 20 show results of cycles to failure for the two cases studied, concluding that the actual material's plane-strain fracture toughness must be greater than the lower-bound value. Figure 19 and Figure 21 show the critical flaw size for a given K_{Ic} for each case.

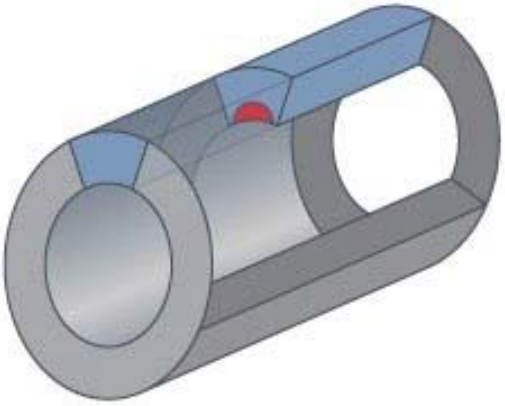

Figure 16 – Circumferential surface flaw, semi-elliptical shape (i.e., thumbnail).

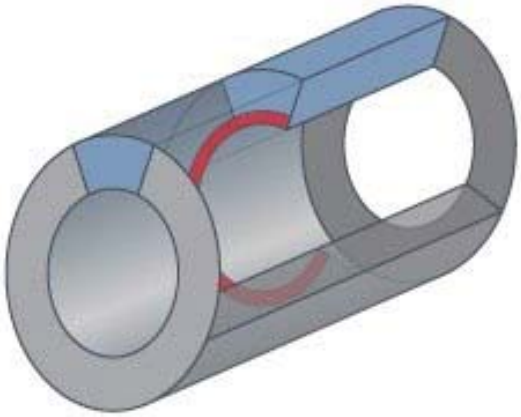

Figure 17 – Circumferential surface flaw, 360° around circumference.

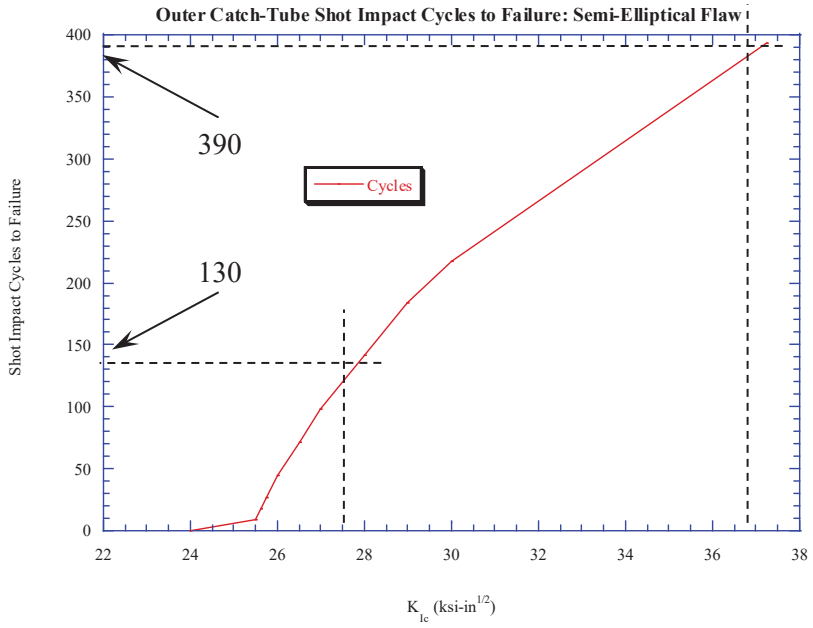

Figure 18 – Case #1: OCT shot impact cycles-to-failure: Circumf., semi-elliptical, surface flaw.

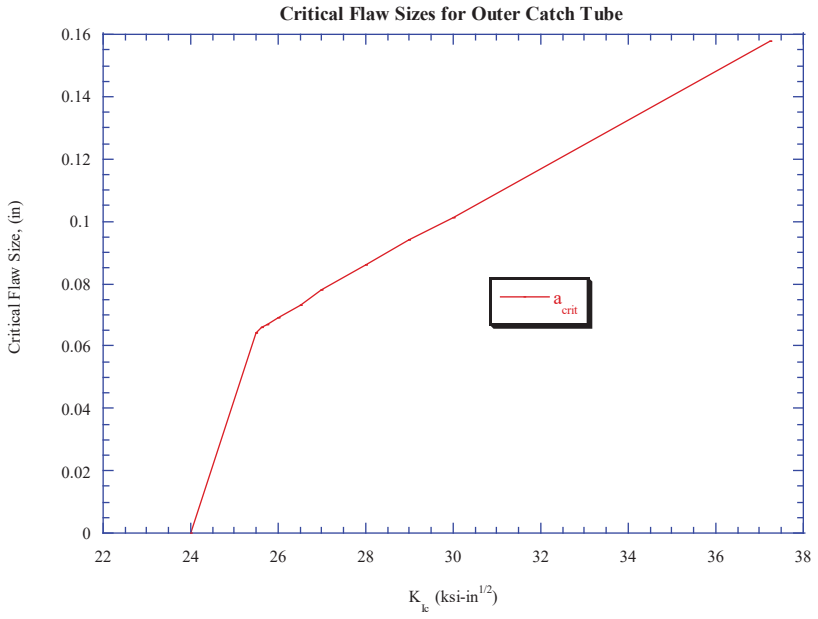

Figure 19 – Case #1: OCT critical flaw size: Circumf., semi-elliptical, surface flaw.

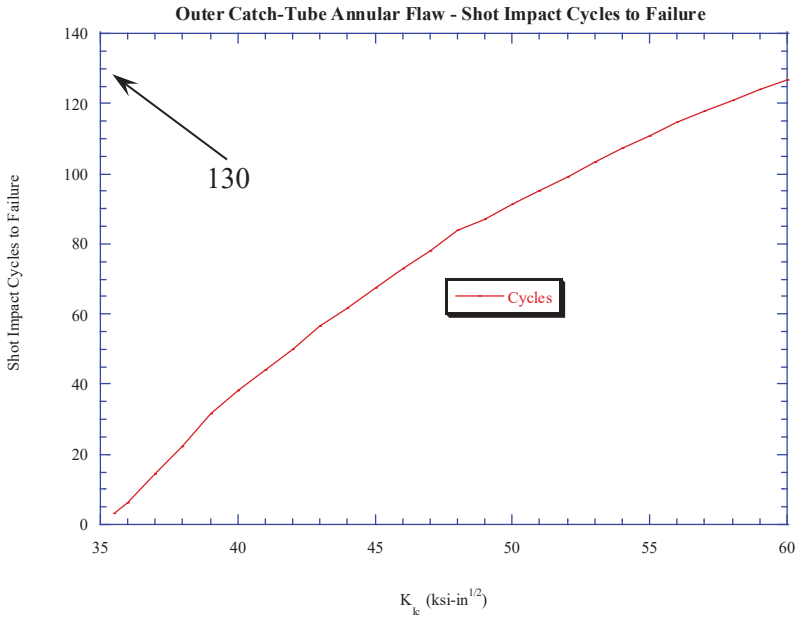

Figure 20 – Case #2: OCT shot impact cycles-to-failure: Annular surface flaw, 360° Circumf.

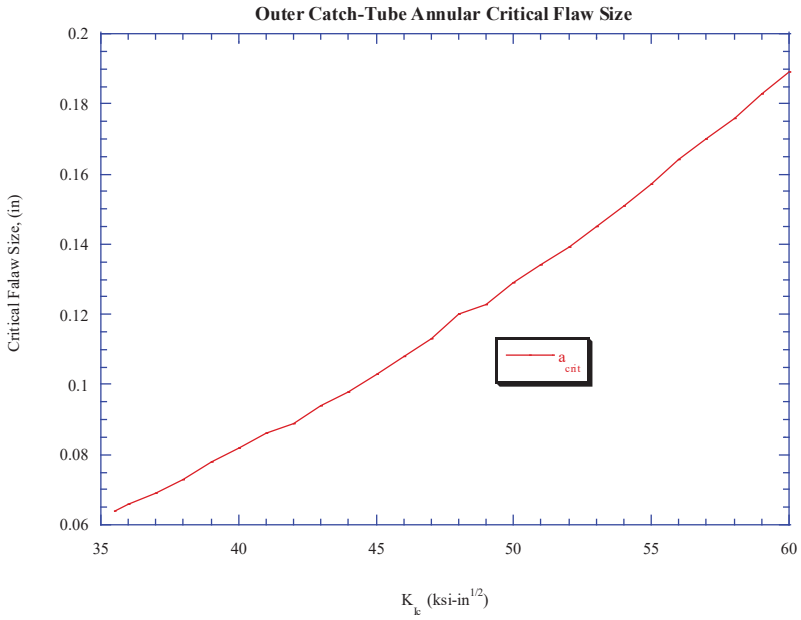

Figure 21 – Case #2: OCT critical flaw size: Annular surface flaw, 360° circumf.

Case #1: For the lower-bound K_{Ic} value of 24 ksi-in$^{1/2}$ given in Table 5, **immediate brittle failure is predicted for the initial shot at 200 m/s velocity for H-11 and H-13 steels**, as shown in Figure 18. Furthermore, spanning a significant number of shot cycles and given the recommended initial flaw size per ASME Code, Sec. VIII, Div. 3, fracture is predicted to occur for a range of K_{Ic} values above the lower-bound. However, predicted critical flaws are larger than the limit of UT detection specified by the ASME Code, implying that flaws larger than Code limit would be detected and removed after non-destructive examination (NDE) process.

Therefore, as long as the fracture toughness is well above the lower-bound of 24 ksi-in$^{1/2}$ it does not appear that brittle fracture would occur for either H-11 or H-13 **under a "one-time" application of load**. Nonetheless, for multiple shot sequences, and based on the historical perspective of 390 total shots (i.e., ~130 shots per outer catch-tube design), the MHW OCT design would require the material toughness to be >30 ksi-in$^{1/2}$ to exceed 130 shot cycles. The magnitude of $K_{Ic} = 30$ correlates to a CVN value ~9 ft-lb. Thus, it is imperative to obtain an actual CMTRs for this particular material lot to determine whether CVN is met or exceeded.

If, however, OCT's are manufactured from 4340 alloy steel exhibiting plane-strain fracture toughness that is potentially twice the magnitude of H-11 and H-13 steel (see Table 7), then many more cycles-to-failure would be available.

Case #2: An annular (i.e., 360° circumferential) flaw would be something that might occur during the manufacturing process, which has been observed in many other applications. This particular flaw assumption might not be something the IFIT component has been subjected to during manufacture, but it does present a worst-case condition that might be undetected during initial NDT examination. At the lower-bound plane-strain fracture toughness of 24 ksi-in$^{1/2}$ for H-11 and H-13, failure is predicted immediately on the first shot. Depending on the plane-strain fracture toughness magnitude, failure is predicted after a certain number of shot cycles, for critical crack depth shown in Figure 21. Yet, it is evident that the plane-strain fracture toughness must be >60 ksi-in$^{1/2}$ to exceed 130 shot cycles. Because LANL has historical evidence of possibly greater than 130 shots for this particular outer catch-tube design, and assuming that further detailed NDE have been performed at regular intervals between shots, then it follows that this particular flaw assumption has not been observed by operators or NDE technicians.

7.0 REDUCED IMPACT VELOCITY RESULTS

LANL project management requested a determination of the impact velocity that, given existing and undetected flaws, would provide stable fatigue crack-growth without complete failure of the OCT component for multiple re-use. As such, similar analyses as performed in Section 6 of this report were repeated to determine cycles to failure at reduced impact velocities assuming the lower-bound plane-strain fracture toughness, K_{Ic}, of 24 ksi-in$^{1/2}$.

Principal stresses developed upon impact on the OCT are assumed as a linear function of the kinetic energy, thus a stress ratio is computed for successive reduced velocities. Table 8 illustrates the OCT cycles-to-failure for the 12.7 kg OPC mass at reduced impact velocities for both flaw assumptions described in Section 6, while using the lower-bound plane-strain fracture toughness for H-11 and H-13. It is assumed that with each shot event, the OCT dynamically reverberates approximately 10 full-amplitude cycles, which must be considered in the overall stress history for fatigue crack-growth.

In accordance with ASME Boiler and Pressure Vessel Code, Section VIII, Division 3 [Ref. 8 and Ref. 9], acceptance standards for linear indications on material thickness greater than 2-inch thick are 3/16-inch long with a 3:1 aspect ratio of length-to-depth of flaw. Thus, 1/16-inch deep by 3/16-inch long flaw is the limiting size. However, NDE surface techniques such as visual (VT), magnetic particle (MT), and liquid penetrant (PT) or volumetric techniques such as ultrasonic (UT) and radiography (RT), might be able to detect smaller flaw sizes than recommended by the ASME Code. As such, it's important that NDE staff examining OCTs be able to understand the bounds of detection capability.

Table 8 shows that for a thumbnail flaw (i.e., circumferential, semi-elliptical flaw) of 1/16-inch deep by 3/16-inch long, failure occurs at 200 m/s impact velocity, but at 190 m/s it would require 87 shots to cause fatigue crack-growth failure. Likewise, at 175 m/s velocity, it would require 615 total shots to cause fatigue crack-growth failure. A typical failure assessment diagram (FAD) is shown in Figure 22 depicting the interaction between ductile failure and brittle fracture.

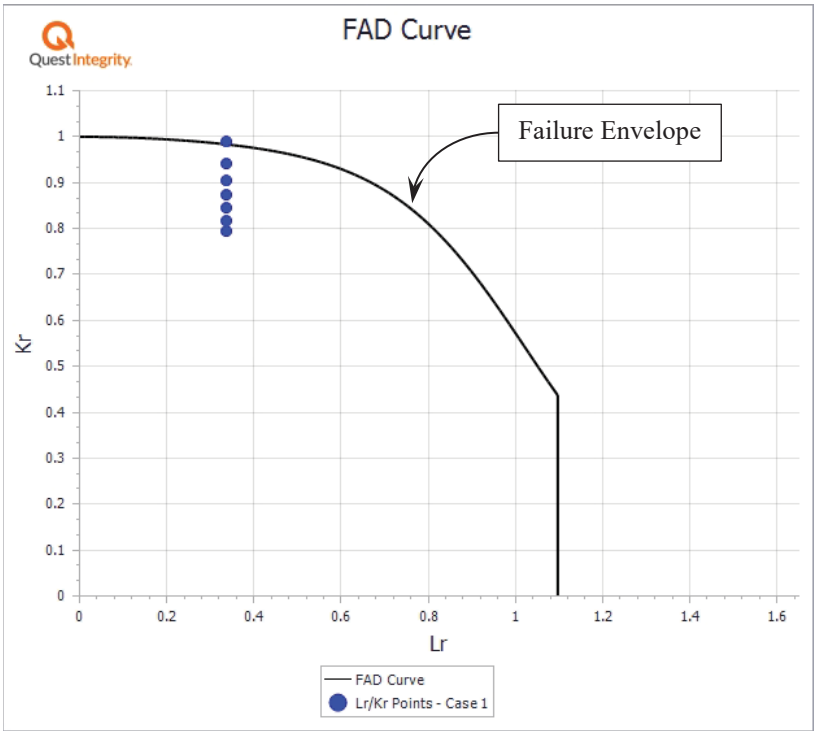

Figure 22 – FAD for fatigue-crack growth of OCT flaw under 175 m/s impact velocity.

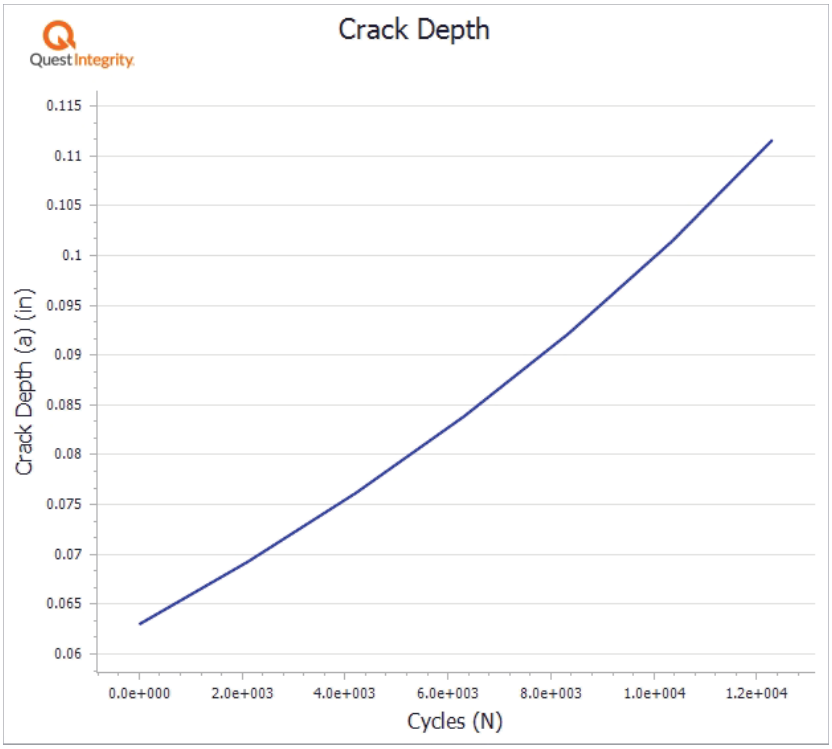

Figure 23 – Crack growth of OCT under 175 m/s impact velocity.

For the annular flaw in H-11 or H-13 steel, which is considered a severe condition from the manufacturing process, immediate failure after a single shot occurs even for impact velocities of 170 m/s. At a reduced impact velocity of 160 m/s, fatigue crack-growth failure is predicted after 95 shots, and approximately 360 shots are required to cause failure for an impact velocity of 150 m/s. Again, as stated previously, the annular flaw is a severe condition that would more than likely have been identified immediately after manufacturing or during initial NDT examinations.

If 4340 alloy steel is used for the OCT, with the associated fracture toughness as listed in Table 7 (which is typically twice that of H-11 and H-13 steel), then failure would not occur at 200 m/s. Additional computations may be developed, if necessary, to determine the cycles-to-failure for 4340 alloy with heat treatment in the range of HRC 40 to 44.

Table 8 – OCT cycles-to-failure; Reduced Impact Velocity for 12.7 kg OPC Mass – Case #1

			Thumbnail Flaw				Annular Flaw			
Velocity	**Kinetic Energy**	**Stress Ratio**	**Crit. Crack**	**N**	**(N/2)**	**(N_{ASME}/10)**	**Crit. Crack**	**N**	**(N/2)**	**(N_{ASME}/10)**
(m/s)	**(kg-m^2/s^2)**	**(ksi)**	**(in)**	**(cycles)**	**(cycles)**	**(cycles)**	**(in)**	**(cycles)**	**(cycles)**	**(cycles)**
200	254000	70.0	Failure				Failure			
190	229235	63.2	0.072	1746	873	87	Failure			
180	205740	56.7	0.100	8305	4153	415	Failure			
175	194469	53.6	0.112	12301	6151	615	Failure			
170	183515	50.6	0.125	17573	8787	879	Failure			
160	162560	44.8	0.163	34637	17319	1732	0.073	1919	960	96
150	142875	39.4	0.210	63861	31931	3193	0.094	7384	3692	369
140	124460	34.3	0.285	118463	59232	5923	0.126	18269	9135	913
130	107315	29.6	0.385	216060	108030	10803	0.170	38977	19489	1949
125	99219	27.3	0.460	297903	148952	14895	0.202	56795	28398	2840
120	91440	25.2	0.548	405966	202983	20298	0.239	80938	40469	4047
115	83979	23.1	0.648	561009	280505	28050	0.29	117096	58548	5855
110	76835	21.2	0.748	764285	382143	38214	0.347	165647	82824	8282

N = Calculated cycles to failure

N/2 = N_{ASME} = ASME Code required factor on cycles

N_{ASME}/10 = Actual cycles to failure accounting for 10 vibration cycles per shot

8.0 DIFFERENT PROJECTILES

The IFIT project has executed over 390 launch shots with different OPC mass, as shown by the abbreviated list in Appendix D. Two separate conditions are also expected to be exercised in the IFIT over the near-term and long-term;

(a) 25 kg OPC mass and

(b) modify use of OPC from Aluminum 6061-T6 to Naval Brass.

8.1 25 kg Mass

As shown in Appendix D, *Launcher Shot Records*, an abbreviated list of 390 shots is provided whose OPC mass range from 12.5 kg to 25.2 kg. A simple kinetic energy ratio is applied, such that a one-to-one correspondence is achieved with the 12.7 kg OPC mass at 200 m/s.

Table 9 provides a listing of OCT cycles-to-failure for the 25 kg aluminum OPC mass at reduced impact velocities. Graphical results are shown in Figure 27 and Figure 28 for the aluminum OPC with respective mass of 12.7 kg and 25 kg.

Table 9 – OCT cycles-to-failure; Reduced Impact Velocity for 25 kg OPC – Case #2

			Thumbnail Flaw				Annular Flaw			
Velocity	Kinetic Energy	Stress Ratio	Crit. Crack	N	(N/2)	(N_{ASME}/10)	Crit. Crack	N	(N/2)	(N_{ASME}/10)
(m/s)	(kg-m^2/s^2)	(ksi)	(in)	(cycles)	(cycles)	(cycles)	(in)	(cycles)	(cycles)	(cycles)
140	245000	67.5	Failure				Failure			
138	238050	65.6	0.064	228	114	11	Failure			
130	211250	58.2	0.092	6388	3194	319	Failure			
120	180000	49.6	0.130	19699	9850	985	Failure			
115	165313	45.6	0.155	31312	15656	1566	0.071	1398	699	70
110	151250	41.7	0.188	49109	24555	2455	0.084	4579	2290	229
100	125000	34.4	0.280	116382	58191	5819	0.126	18096	9048	905
90	101250	27.9	0.438	273293	136647	13665	0.195	51896	25948	2595
80	80000	22.0	0.698	668150	334075	33408	0.321	142894	71447	7145
70	61250	16.9	1.110	1704388	852194	85219	0.554	396730	198365	19837

8.2 Brass vs Aluminum Projectile

Outer projectile cylinders for the IFIT are considered “one-time use” components manufactured from aluminum 6061-T6, as shown in Figure 24 and Figure 25. Furthermore, LANL management would like to modify the material to brass, which has a density increase of ~ 3 times that of aluminum.

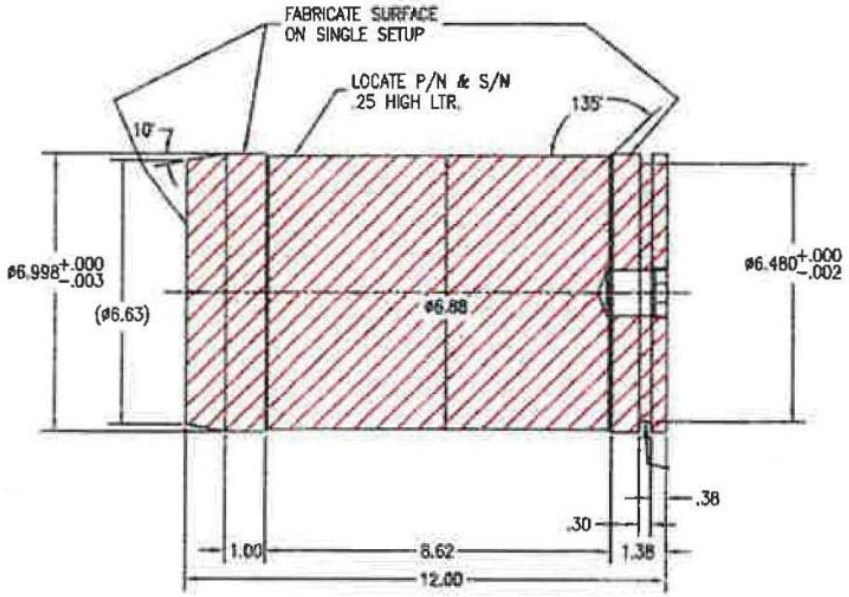

Figure 24 – Solid outer projectile cylinder.

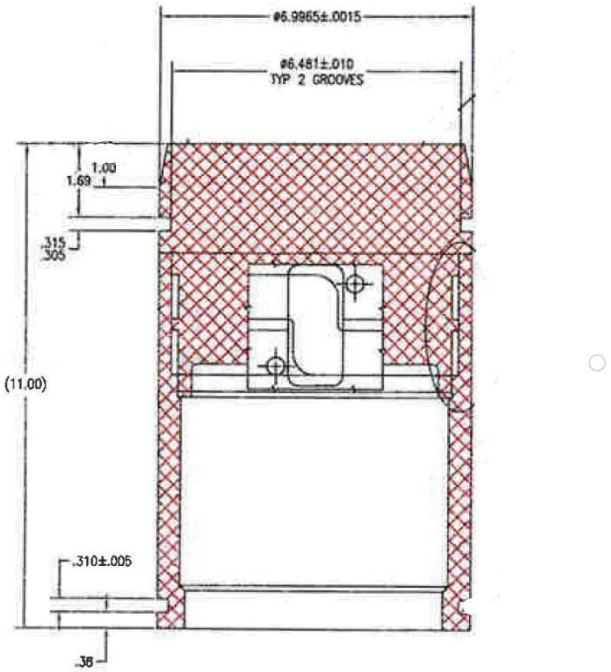

Figure 25 – MHW water-cooled outer projectile cylinder.

Again, a simple kinetic energy ratio may be applied herein thereby increasing the overall mass of OPC (i.e., 12.7 kg or 25 kg mass). The original analysis performed by W-13 utilized an aluminum OPC of 12.7 kg mass. Thus, the four cases analyzed here are shown in Figure 26.

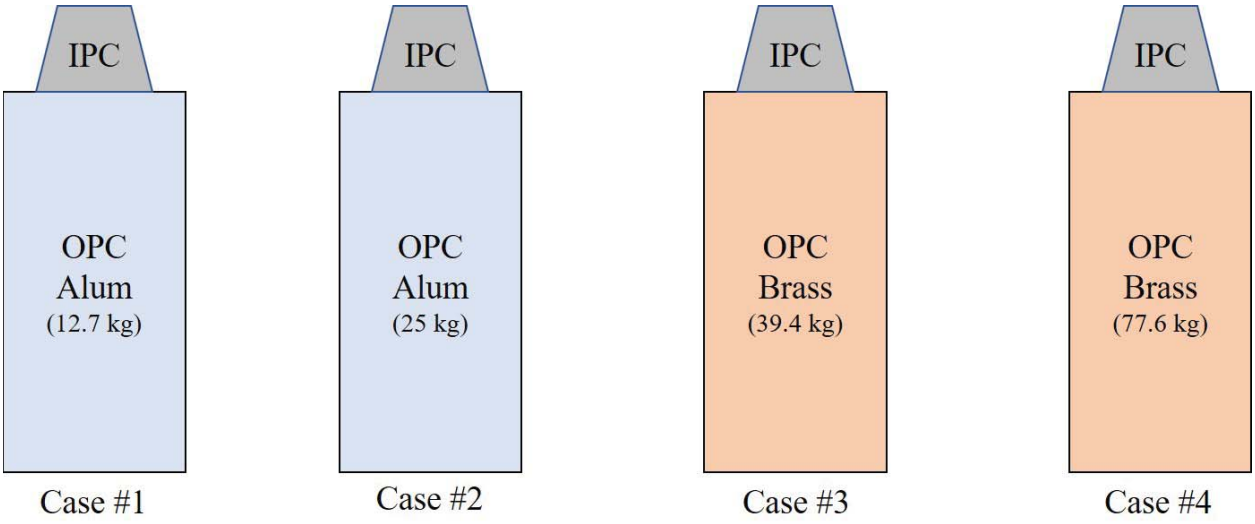

Figure 26 – Four separate OPC component mass.

Mass density of aluminum and brass are taken from the ASME Code [9] and listed in Table 10.

Table 10 – OPC Material Density

Material	Density (lb/in^3)	Notes
Aluminum	0.098	6061-T6
Brass	0.304	Naval brass

Density Ratio (Brass/Alum) = 3.10204

Based on LANL drawing geometry, the total mass of OPC for the four cases shown in Figure 26 are listed below in Table 11.

Table 11 – Total Mass of Case#1 through Case #4 Assemblies

OPC Mass	OPC Mass (kg)	OPC Mass (lb)
Case #1	12.7	28
Case #2	25	55
Case #3	39.4	87
Case #4	77.6	171

Table 12 – OCT cycles-to-failure; Reduced Impact Velocity for 39.4 kg Brass OPC – Case #3

			Thumbnail Flaw				Annular Flaw			
Velocity	Kinetic Energy	Stress Ratio	Crit. Crack	N	(N/2)	(N_{ASME}/10)	Crit. Crack	N	(N/2)	(N_{ASME}/10)
(m/s)	(kg-m^2/s^2)	(ksi)	(in)	(cycles)	(cycles)	(cycles)	(in)	(cycles)	(cycles)	(cycles)
113.55	254004	70.0	Failure				Failure			
110	238370	65.7	0.064	227	114	11	Failure			
105	217193	59.9	0.086	4689	2345	234	Failure			
100	197000	54.3	0.108	11075	5538	554	Failure			
95	177793	49.0	0.135	21427	10714	1071	Failure			
93	170385	47.0	0.148	27026	13513	1351	0.066	448	224	22
90	159570	44.0	0.168	37711	18856	1886	0.076	2474	1237	124
80	126080	34.7	0.275	112172	56086	5609	0.122	16963	8482	848
70	96530	26.6	0.485	329305	164653	16465	0.214	64014	32007	3201
65	83233	22.9	0.648	577140	288570	28857	0.296	121512	60756	6076
60	70920	19.5	0.873	1031689	515845	51584	0.416	230607	115304	11530

Table 13 – OCT cycles-to-failure; Reduced Impact Velocity for 77.6 kg Brass OPC – Case #4

			Thumbnail Flaw				Annular Flaw			
Velocity	Kinetic Energy	Stress Ratio	Crit. Crack	N	(N/2)	(N_{ASME}/10)	Crit. Crack	N	(N/2)	(N_{ASME}/10)
(m/s)	(kg-m^2/s^2)	(ksi)	(in)	(cycles)	(cycles)	(cycles)	(in)	(cycles)	(cycles)	(cycles)
80.92	254064	70.0	Failure				Failure			
80	248320	68.4	Failure				Failure			
78	236059	65.1	0.066	463	232	23				
77	230045	63.4	0.072	1728	864	86				
75	218250	60.1	0.084	4343	2172	217	Failure			
70	190120	52.4	0.116	14086	7043	704	Failure			
66	169013	46.6	0.15	28262	14131	1413	0.067	681	341	34
65	163930	45.2	0.160	33184	16592	1659	0.072	1654	827	83
60	139680	38.5	0.223	71370	35685	3569	0.100	8848	4424	442
55	117370	32.3	0.323	152038	76019	7602	0.142	25266	12633	1263
50	97000	26.7	0.485	325300	162650	16265	0.214	63236	31618	3162
40	62080	17.1	1.098	1637848	818924	81892	0.542	379757	189879	18988

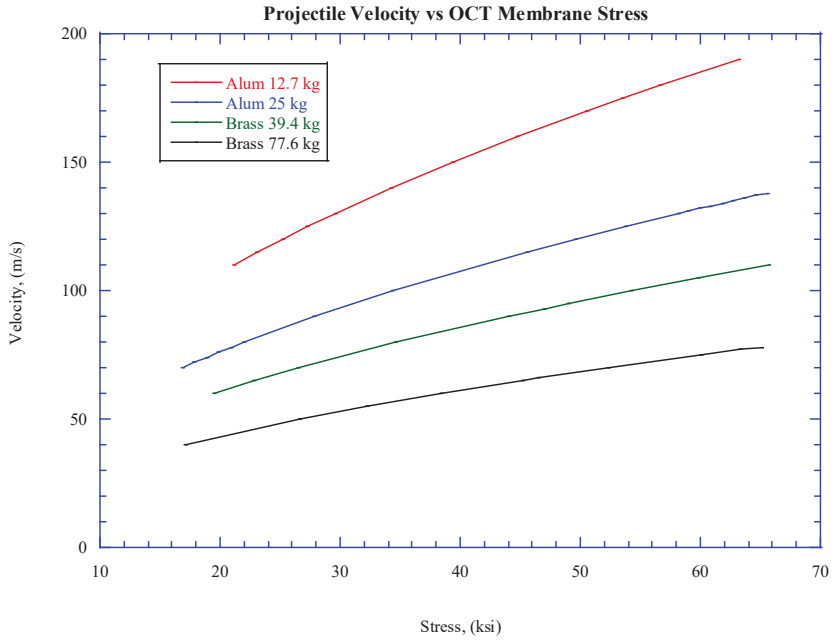

Figure 27 – Projectile velocity as a function of OCT membrane stress – Thumbnail Flaw.

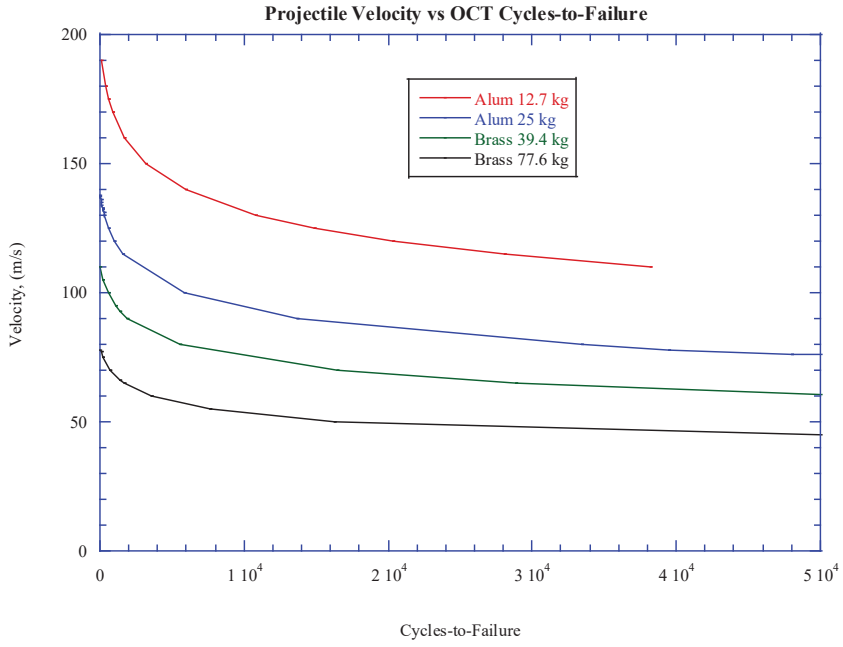

Figure 28 – Projectile velocity as a function of OCT shot cycles to failure – Thumbnail Flaw.

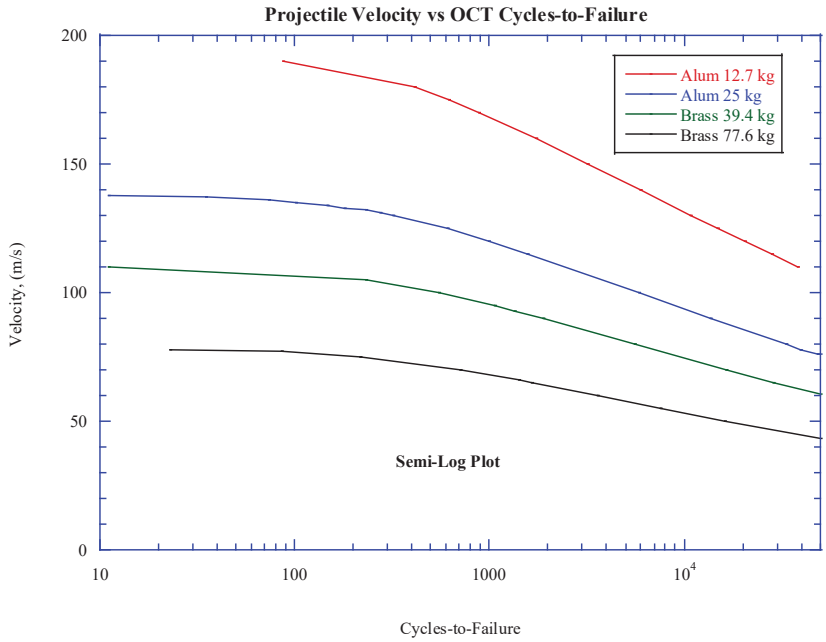

Figure 29 – Projectile velocity as a function of OCT shot cycles to failure – Thumbnail Flaw.

9.0 CONCLUSION

Analysis of H-11 VAR and H-13 VAR ultrahigh strength steel IFIT outer catch-tube sub-assembly shows that the largest surface-flaw that might be undetected by UT inspection will not propagate unstably under the dynamic impact stresses generated for a single shot sequence, assuming the material plane-strain fracture toughness, K_{Ic}, exceeds ~30 ksi-in$^{1/2}$, or likewise, exceeds a CVN of 9 ft-lb, for the OPC mass of 12.7 kg at a velocity of 200 m/s. Because 4340 alloy steel has a much higher fracture toughness, about a factor of 2 higher than H-11 and H-13, no fatigue crack-growth has been performed and is assumed herein to be acceptable.

The maximum primary stress, uniformly distributed across the thickness, shows that a 3/16" long thumbnail flaw with 3:1 aspect ratio (i.e., length-to-depth) attains a stress intensity factor at the crack-tip slightly lower than the plane-strain fracture toughness, K_{Ic}, of 30 ksi-in$^{1/2}$. However, there is no CMTR information relative to the notch toughness or fracture toughness of the actual OCT material. That stated, a minimum value of the fracture toughness of 24 ksi-in$^{1/2}$ has been applied to the fracture mechanics calculations (see Section 6) for H-11 and H-13 steel. Given this lower fracture toughness, brittle failure is predicted for both flaw types addressed herein after a single shot at 200 m/s impact velocity. Again, 4340 steel presumably having a fracture toughness of twice that H-11 and H-13, would nonetheless be acceptable and attain much higher cycles-to-failure.

A reduced impact velocity fatigue crack-growth analysis has been performed for both flaw types described in Section 6 to determine the impact velocity, below which, many more shot executions can be performed. That is, with the minimum specified plane-strain fracture toughness of 24 ksi-in$^{1/2}$ for H-11 and H-13, a set of computations were performed to determine the maximum velocity where additional shot cycles may be performed. Table 6 provides the data supporting the fatigue crack-growth conditions for each flaw type for H-11 and H-13 steel. As stated earlier, 4340 alloy steel has a factor of 2 higher fracture toughness and therefore no analysis was performed. As shown in Table 8 for the circumferential, semi-elliptical flaw (i.e., thumbnail flaw), the OCT component is capable of 87 shot executions at a maximum impact velocity of 190 m/s. The annular flaw, which is much more severe condition, the OCT is capable of 96 shots at a maximum impact velocity of 160 m/s.

Lastly, different outer projectile cylinder mass based on either aluminum or brass have been addressed. This was accomplished by modifying the mass and associated kinetic energy to allow for both a 12.7 kg and 25 kg aluminum OPC, and 39.4 kg and 77.6 kg brass OPC. Results are shown in Figure 27 and Figure 28, depicting the number of shot cycles to failure for the respective OPC material. Figure 29 is semi-log plot for ease of visualization at the lower cycle-to-failure end of the curve. These charts will aid IFIT staff in determining re-use of OCTs given a specific OPC material and mass.

10. RECOMMENDATIONS

The following recommendations are provided to ensure that the materials utilized for the OCT designs are capable of performing as required.

a) CMTRs: Must be provided for all new materials. Data must include:
   i. material chemistry,
   ii. tensile limits (yield strength, ultimate strength),
   iii. ductility measures (% elongation, % reduction of area) and
   iv. impact toughness (CVN).

   CMTR data will validate those material properties used in this evaluation.

b) NDE Limits: For the material or component being examined, limits of detectability for flaw sizes should be determined from the respective examination method, VT, RT, UT, MT or PT. This might reduce the as-recommended flaw size for engineering evaluations.
c) Max Flaw Size: Currently, the allowable flaw size is based on guidance stipulated in ASME Code, Sec. VIII, Div. 3 [9]. Specific NDE techniques might be able to capture smaller surface or subsurface indications than used herein, and thus be able to increase OCT cycles-to-failure.
d) NDE Inspection Intervals: IFIT project management stated that OCT components are visually examined (VT) after every shot cycle. If surface indications are observed during the VT examination, a further NDE examination technique utilizing MT or PT should be performed to determine actual flaw size, and compare against ASME recommended flaw sizes utilized in this analysis.

11.0 REFERENCES

1. LANL Dwg. 55Y-002782, "IFIT Catch Tube Assemblies; Milli-Watt, Multi-hundred Watt and GPHS Outer Catch Tube," Rev. 6, Sheets 1 through 25, February 27, 2015.

2. Crane, D., "Structural Assessment of the Isotope Fuel Impact Tester (IFIT) Catch Tube Subassembly," Los Alamos National Laboratory, Weapon Systems Engineering, LA-UR-09-08155.

3. Art Herrera e-mail to Ben Lopez, Subject: "Reuse of IFIT Outer Catch Tubes," September 27, 2016.

4. CINDAS, Center for Information and Numerical Data Analysis and Synthesis, "Aerospace Structural Metals Database & High-Performance Alloys Database," West Lafayette, IN, 2016.

5. ASM, ***Metals Handbook Desk Edition***, 2nd edition, "Structure/Property Relationships in Irons and Steels," pp. 153-173, ASM International, 1998.

6. DeFries, R. S., "Estimation of Yield Strength from Hardness Measurements," WVT-TN-75051, Benet Weapons Laboratory, Watervliet Arsenal, NY., August 1975.

7. Rodriguez, E., "Elastic-Plastic Constitutive Material Models for Numerical Simulations," Los Alamos National Laboratory, DynEx Vessel Project, DV-CAL-0068, Rev. 0, March 2004.

8. ASME, "Code Case 2564 - Impulsively Loaded Pressure Vessels," Rev. 5, American Society of Mechnaical Engineers, March 24, 2016.

9. ASME. "Alternative Rules for Construction of High-Pressure Vessels," Section VIII, Division 3, American Society of Mechanical Engineers, 2015.

10. Blevins, R. D., ***Formulas for Natural Frequency and Mode Shape***, Krieger Publishing Company, Ft. lauderdale, FL, 1993.

11. Biggs, J. M., ***Introduction to Structural Dynamics***, McGraw-Hill Publishing Company, New York, NY, 1964.

12. API/ASME, "Fitness for Service," API 579-1/ASME FFS-1, American Petroleum Institute (API) and American Society of Mechanical Engineers (ASME), June 2016.

13. Rodriguez, E. A., "Engineering Analysis, Gemini Experimental Series, Evaluation of 3-ft Diameter HSLA-100 Spherical Confinement Vesse's Conformance to ASME B&PV Code,

Section VIII, Division 3, and Code Case 2564-2," Los Alamos National Laboratory, W-14-TR-0043U, Rev. B, Feb. 2012.

14. Duffey, T. A., "Plastic Instabilities in Spherical Vessels for Static and Dynamic Loading," Journal of Pressure Vessel Technology, Vol. 133 (5) 051210, July 2011.

15. Barsom, J. M., and Rolfe, S. T, ***Fracture and Fatigue Control in Structures; Applications of Fracture Mechanics***, 2nd Edition, Prentice Hall Inc. Publishing, New York, NY, 1987.

16. Leskovšek, V., "Correlation Between K_{Ic} , HRC and Charpy V-Notch Test Results for H11/H13 Hotwork Tool Steels at Room Temperature," Steel Reasearch International, Vol. 79 No. 4, 2008, pp. 306-313.

17. Quest Integrity, LLC, "SIGNAL-FFS; Fitness-for-Service," Version 4.0, 2015.

APPENDIX A – Hardness Conversion Chart

Rockwell						Rockwell Superficial				Brinell		Vickers	Shore	
A	B	C	D	E	F	15-N	30-N	45-N	30-T	3000 kg	500 kg	136		Approx Tensile Strength (psi)
60kg Brale	100kg 1/16" Ball	150kg Brale	100kg Brale	100kg 1/8" Ball	60kg 1/16" Ball	15kg Brale	30kg Brale	45kg Brale	30 kg 1/16" Ball	10mm Ball Steel	10mm Ball Steel	Diamond Pyramid	Sciero-scope	
86.5	---	70	78.5	---	---	94.0	86.0	77.6	---	---	---	1076	101	---
86.0	---	69	77.7	---	---	93.5	85.0	76.5	---	---	---	1044	99	---
85.6	---	68	76.9	---	---	93.2	84.4	75.4	---	---	---	940	97	---
85.0	---	67	76.1	---	---	92.9	83.6	74.2	---	---	---	900	95	---
84.5	---	66	75.4	---	---	92.5	82.8	73.2	---	---	---	865	92	---
83.9	---	65	74.5	---	---	92.2	81.9	72.0	---	739	---	832	91	---
83.4	---	64	73.8	---	---	91.8	81.1	71.0	---	722	---	800	88	---
82.8	---	63	73.0	---	---	91.4	80.1	69.9	---	705	---	772	87	---
82.3	---	62	72.2	---	---	91.1	79.3	68.8	---	688	---	746	85	---
81.8	---	61	71.5	---	---	90.7	78.4	67.7	---	670	---	720	83	---
81.2	---	60	70.7	---	---	90.2	77.5	66.6	---	654	---	697	81	320,000
80.7	---	59	69.9	---	---	89.8	76.6	65.5	---	634	---	674	80	310,000
80.1	---	58	69.2	---	---	89.3	75.7	64.3	---	615	---	653	78	300,000
79.6	---	57	68.5	---	---	88.9	74.8	63.2	---	595	---	633	76	290,000
79.0	---	56	67.7	---	---	88.3	73.9	62.0	---	577	---	613	75	282,000
78.5	120	55	66.9	---	---	87.9	73.0	60.9	---	560	---	595	74	274,000
78.0	120	54	66.1	---	---	87.4	72.0	59.8	---	543	---	577	72	266,000
77.4	119	53	65.4	---	---	86.9	71.2	58.6	---	525	---	560	71	257,000
76.8	119	52	64.6	---	---	86.4	70.2	57.4	---	500	---	544	69	245,000
76.3	118	51	63.8	---	---	85.9	69.4	56.1	---	487	---	528	68	239,000
75.9	117	50	63.1	---	---	85.5	68.5	55.0	---	475	---	513	67	233,000
75.2	117	49	62.1	---	---	85.0	67.6	53.8	---	464	---	498	66	227,000
74.7	116	48	61.4	---	---	84.5	66.7	52.5	---	451	---	484	64	221,000
74.1	116	47	60.8	---	---	83.9	65.8	51.4	---	442	---	471	63	217,000
73.6	115	46	60.0	---	---	83.5	64.8	50.3	---	432	---	458	62	212,000
73.1	115	45	59.2	---	---	83.0	64.0	49.0	---	421	---	446	60	206,000
72.5	114	44	58.5	---	---	82.5	63.1	47.8	---	409	---	434	58	200,000
72.0	113	43	57.7	---	---	82.0	62.2	46.7	---	400	---	423	57	196,000

Tensile Strength

Rockwell-C

71.5	113	42	56.9	---	---	81.5	61.3	45.5	---	390	---	412	56	191,000
70.9	112	41	56.2	---	---	80.9	60.4	44.3	---	381	---	402	55	187,000
70.4	112	40	55.4	---	---	80.4	59.5	43.1	---	371	---	392	54	182,000
69.9	111	39	54.6	---	---	79.9	58.6	41.9	---	362	---	382	52	177,000
69.4	110	38	53.8	---	---	79.4	57.7	40.8	---	353	---	372	51	173,000
68.9	110	37	53.1	---	---	78.8	56.8	39.6	---	344	---	363	50	169,000
68.4	109	36	52.3	---	---	78.3	55.9	38.4	---	336	---	354	49	165,000
67.9	109	35	51.5	---	---	77.7	55.0	37.2	---	327	---	345	48	160,000
67.4	108	34	50.8	---	---	77.2	54.2	36.1	---	319	---	336	47	156,000
66.8	108	33	50.0	---	---	76.6	53.3	34.9	---	311	---	327	46	152,000
66.3	107	32	49.2	---	---	76.1	52.1	33.7	---	301	---	318	44	147,000
65.8	106	31	48.4	---	---	75.6	51.3	32.5	---	294	---	310	43	144,000
65.3	105	30	47.7	---	---	75.0	50.4	31.3	---	286	---	302	42	140,000
64.7	104	29	47.0	---	---	74.5	49.5	30.1	---	279	---	294	41	137,000
64.3	104	28	46.1	---	---	73.9	48.6	28.9	---	271	---	286	41	133,000
63.8	103	27	45.2	---	---	73.3	47.7	27.8	---	264	---	279	40	129,000
63.3	103	26	44.6	---	---	72.8	46.8	26.7	---	258	---	272	39	126,000
62.8	102	25	43.8	---	---	72.2	45.9	25.5	---	253	---	266	38	124,000
62.4	101	24	43.1	---	---	71.6	45.0	24.3	---	247	---	260	37	121,000
62.0	100	23	42.1	---	---	71.0	44.0	23.1	82.0	240	201	254	36	118,000
61.5	99	22	41.6	---	---	70.5	43.2	22.0	81.5	234	195	248	35	115,000
61.0	98	21	40.9	---	---	69.9	42.3	20.7	81.0	228	189	243	35	112,000
60.5	97	20	40.1	---	---	69.4	41.5	19.6	80.5	222	184	238	34	109,000
59.0	96	18	---	---	---	---	---	---	80.0	216	179	230	33	106,000
58.0	95	16	---	---	---	---	---	---	79.0	210	175	222	32	103,000
57.5	94	15	---	---	---	---	---	---	78.5	205	171	213	31	100,000
57.0	93	13	---	---	---	---	---	---	78.0	200	167	208	30	98,000
56.5	92	12	---	---	---	---	---	---	77.5	195	163	204	29	96,000
56.0	91	10	---	---	---	---	---	---	77.0	190	160	196	28	93,000
55.5	90	9	---	---	---	---	---	---	76.0	185	157	192	27	91,000
55.0	89	8	---	---	---	---	---	---	75.5	180	154	188	26	88,000
54.0	88	7	---	---	---	---	---	---	75.0	176	151	184	26	86,000
53.5	87	6	---	---	---	---	---	---	74.5	172	148	180	26	84,000
53.0	86	5	---	---	---	---	---	---	74.0	169	145	176	25	83,000
52.5	85	4	---	---	---	---	---	---	73.5	165	142	173	25	81,000
52.0	84	3	---	---	---	---	---	---	73.0	162	140	170	25	79,000
51.0	83	2	---	---	---	---	---	---	72.0	159	137	166	24	78,000
50.5	82	1	---	---	---	---	---	---	71.5	156	135	163	24	76,000
50.0	81	0	---	---	---	---	---	---	71.0	153	133	160	24	75,000
49.5	80	---	---	---	---	---	---	---	70.0	150	130	---	---	73,000

Tensile Strength

Rockwell-C

APPENDIX B - Material Properties for H-13 VAR Steel

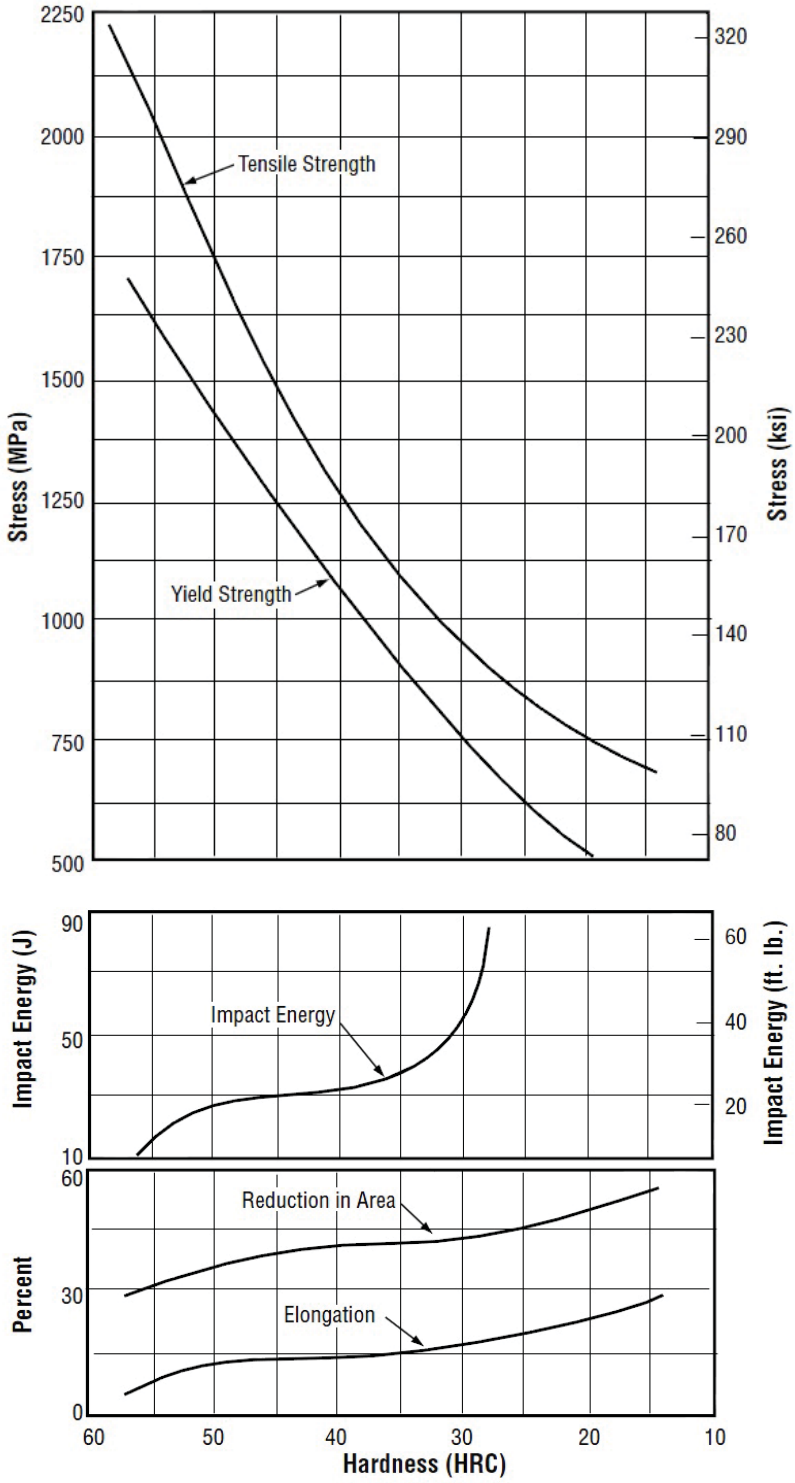

Figure 3.2.1.3 Room temperature tensile properties of H-13 steel in relation to hardness and Charpy V-notch impact energy (Ref. 44)

Table 3.2.1.4 Room temperature tensile properties of annealed and heat treated H-13 steel (Ref. 16)

Condition	Hardness (HRC)	Yield Strength* (ksi)	Ultimate Strength* (ksi)	Elongation* (%)	Reduction of Area* (%)
Annealed	15	54	97	32.0	66.0
Heat treated**	46	204	218	13.0	47.0
Heat Treated**	51	250	281	5.0	10.0

*Standard ASTM 0.505 in. round tensile specimens cut from 1.125 in. bar stock , average of two tests.
**Austenitized at 1825F, air cooled, and double tempered to hardness shown.

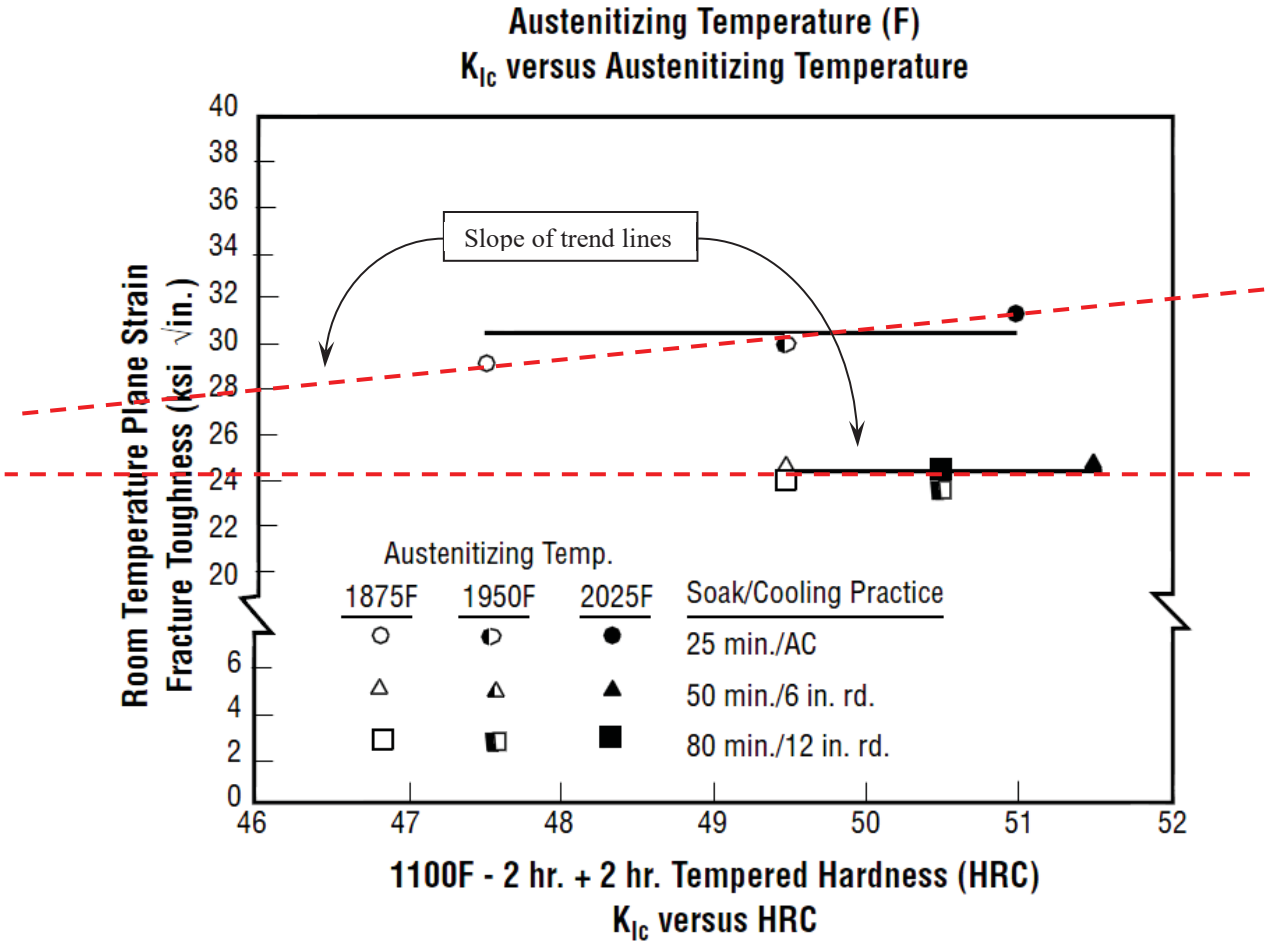

Table 3.2.3.2 Transverse Charpy V-notch impact toughness at room temperature of various grades of H-13 steel at 45–46 HRC (Ref. 43)

Grade	Hardness (HRC)	Transverse Charpy-V Notch Impact Toughness (ft-lb)
Premium Quality H-13	46	10
Conventional Sulfurized H-13	45	2
CPM Nu-Die EZ (Crucible)	45	7-9

Table 3.2.3.1 Longitudinal Charpy V-notch impact properties at room temperature of H-13 bar air cooled from an 1850F austenitizing temperature and tempered at different temperatures (Ref. 1)

Tempering temperature (F)	Hardness (HRC)	Charpy V-notch Impact Energy	
		(ft-lb)	(J)
975	54	10	14
1050	52	10	14
1125	47	18	24
1140	43	18	24

Appendix C – Material Properties for 4340 Steel

MECHANICAL PROPERTIES

	Tensile Strength	Yield Strength	Elongation in 2"	Red. Area	Brinell	Izod
As Rolled	178,000	100,000	10	30	363	—
Annealed	110,000	66,000	23	49	197	25

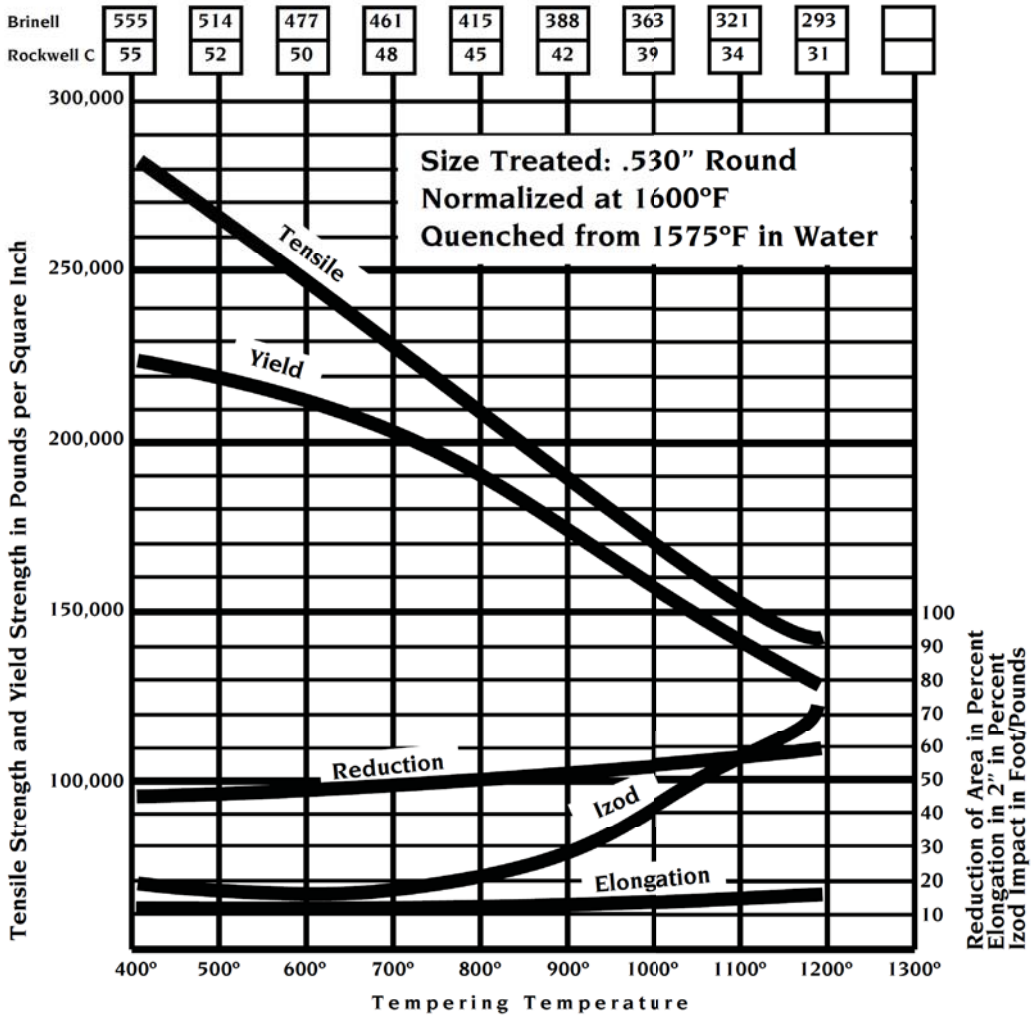

Mechanical properties of selected carbon and alloy steels in the quenched-and-tempered condition

AISI No.[(a)]	Tempering temperature		Tensile strength		Yield strength		Elongation, %	Reduction in area, %	Hardness, HB	Hardness, HRC
	°C	°F	MPa	ksi	MPa	ksi				
4340	205	400	1875	272	1675	243	10	38	520	53
	315	600	1724	250	1586	230	10	40	486	48
	425	800	1469	213	1365	198	10	44	430	46
	540	1000	1172	170	1076	156	13	51	360	39
	650	1200	965	140	855	124	19	60	280	29

Appendix D – Launcher Shot Records

7 Inch Launcher Shot Records *(Records in red indicate $^{238}PuO_2$ shots)*

Run Number	Date	Projectile Weight (Kg)	Breech Pressure (psig)	Sample Number	Test Temp. °C	Test Velocity (m/s)	Thermocouple Type
IFIT-190	30-May-80	12.5	470	mW #MAD-0802-178	450	147.79 +/- .24	Type K (Chromel - Alumel)
IFIT-191	24-Jun-80		153	MHFT-69	825	82.27 +/- .39	Type C (W 5% Re - W 26% Re)
IFIT-192	31-Jul-80		151	MHFT-70	1113	~81.5	Type C (W 5% Re - W 26% Re)
IFIT-193	4-Aug-80		151	MHFT-72	1122	81.57 +/- .27	Type C (W 5% Re - W 26% Re)
IFIT-194	23-Sep-80	25.2	132	IRG-87(Pu) & GCI-35,42,48(U)	820	~58	Type K (Chromel - Alumel)
IFIT-195	25-Sep-80	25.1	132	IRG-88(Pu) & GCI-21,41,70(U)	850	58.39 +/- .13	Type K (Chromel - Alumel)
IFIT-196	1-Oct-80	24.4	126	IRG-89(Pu) & GCI-47(U)	850	58.02 +/- .06	Type K (Chromel - Alumel)
IFIT-197	9-Oct-80	25.1	132	IRG-90(Pu) & GCI-25,39,42(U)	850	~58.3	Type K (Chromel - Alumel)
IFIT-198	31-Oct-80		150	MHFT-68	1215	81.70 +/- .28	Type C (W 5% Re - W 26% Re)
IFIT-199	18-Nov-80	12.8	470	mW #MAD-0026-J77	450	149.05 +/- .26	Type K (Chromel - Alumel)
IFIT-200	20-Nov-80	12.6	470	mW #MAD-0128-K77	450	147.90 +/- .17	Type K (Chromel - Alumel)
IFIT-201	26-Jan-81	12.6	470	mW #LASL 71	450	150.98 +/- .17	Type K (Chromel - Alumel)
IFIT-202	28-Jan-81	12.6	470	mW #LASL 72	450	150.71 +/- .31	Type K (Chromel - Alumel)
IFIT-203	30-Jan-81		150	MHFT-74	1120	80.55 +/- .09	Type C (W 5% Re - W 26% Re)
IFIT-204	5-Feb-81		150	MHFT-75	1120	80.49 +/- .04	Type C (W 5% Re - W 26% Re)
IFIT-205	11-Feb-81	12.5	470	mW #UAS-010T-H80	450	149.73 +/- .24	Type K (Chromel - Alumel)
IFIT-206	13-Feb-81		470	mW #UAS-011T-H80	450	150.44 +/- .10	Type K (Chromel - Alumel)
IFIT-207	25-Feb-81	12.6	470	mW #UAS-013T	450	149.81 +/- .08	Type K (Chromel - Alumel)
IFIT-208	30-Apr-81	24.9	130	4 Copper Pellets		58.66 +/- .08	
IFIT-209	4-May-81	23.9	123	None		59.18 +/- .14	
IFIT-210	21-May-81	24.9	123	IRG-101,102,105&104(Pu)	930	57.04 +/- .18	Type K (Chromel - Alumel)
IFIT-211	30-Jul-81		500	Encapsulated Thoria Powder	Ambient	151.61 +/- .20	Type K (Chromel - Alumel)
IFIT-212	24-Aug-81	12.6	470	mW #UAS-0006-H81	450	150.21 +/- .39	Type K (Chromel - Alumel)
IFIT-213	28-Aug-81		150	MHFT-71	1105	81.58 +/- .06	Type C (W 5% Re - W 26% Re)
IFIT-214	29-Sep-81	22.7	83	RHU # RU-9-02		49.26 +/- .06	Type K (Chromel - Alumel)
IFIT-215	1-Oct-81		125	SR-105,106,107&110	967	~58	Type K (Chromel - Alumel)
IFIT-216	13-Oct-81		83	RHU - RU-31 #22	50	~49	Type K (Chromel - Alumel)
IFIT-217	14-Oct-81		83	RHU # 23	47	49.3 +/- .20	Type K (Chromel - Alumel)
IFIT-218	15-Oct-81	22.6	83	RHU # 24	52	49.58 +/- .06	Type K (Chromel - Alumel)
IFIT-219	15-Dec-81	12.6	470	mW #MAD-0108	450	150.14 +/- .13	Type K (Chromel - Alumel)
IFIT-220	23-Feb-82	14.6	151	MHFT-73	1090	81.59 +/- .09	Type C (W 5% Re - W 26% Re)